Science of the Total Environment 744 (2020) 140714

Contents lists available at ScienceDirect

Science of the Total Environment

journal homepage: www.elsevier.com/locate/scitotenv

Review

Influences of feedstock sources and pyrolysis temperature on the properties of biochar and functionality as adsorbents: A meta-analysis

Masud Hassan [a,b], Yanju Liu [a,b,*], Ravi Naidu [a,b], Sanjai J. Parikh [c], Jianhua Du [a,b], Fangjie Qi [a,b], Ian R. Willett [d]

[a] Global Centre for Environmental Remediation, Faculty of Science, University of Newcastle, Callaghan, NSW 2308, Australia
[b] Cooperative Research Centre for Contamination Assessment and Remediation of the Environment (CRC CARE), Callaghan, NSW 2308, Australia
[c] Department of Land, Air and Water Resources, University of California, Davis, CA, USA
[d] School of Agriculture & Food, The University of Melbourne, VIC 3052, Australia

HIGHLIGHTS

- Pyrolysis temperature, feedstocks types significantly influence properties of biochar.
- Wood derived biochars have high biochar yield and stability than grass and manure derived biochar.
- Manure and grass derived biochar produces more ash content and high pH than wood-derived biochar.
- Electrostatic interactions occur among ionic contaminants and hydrophilic biochar.
- Non-polar interaction occurs among organic contaminants and hydrophobic biochars.

GRAPHICAL ABSTRACT

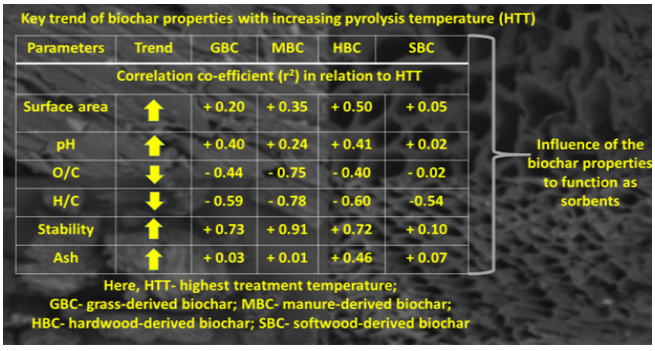

ARTICLE INFO

Article history:
Received 24 April 2020
Received in revised form 1 July 2020
Accepted 1 July 2020
Available online 12 July 2020

Editor: Jay Gan

Keywords:
Biochar
Pyrolysis
Polarity
Functional group
Contaminant
Adsorption

ABSTRACT

Biochar is a porous, amorphous, stable, and low-density carbon material derived from the carbonization of various biological residues. Biochars have multifunctional properties that make them promising adsorbents for the remediation of organic and inorganic contaminants from soil and water. High temperature treatment (HTT) and the properties of feedstocks are key factors influencing the properties of biochars. Feedstocks have distinctive physicochemical properties due to variations in elemental and structural composition, and they respond heterogeneously to specific pyrolysis conditions. The criteria for the selection of feedstocks and pyrolysis conditions for designing biochars for specific sorption properties are inadequately understood. We evaluated the influence of pyrolysis temperature on a wide range of feedstocks to investigate their effects on biochar properties. With increasing HTT, biochar pH, surface area, pore size, ash content, hydrophobicity and O/C vs. H/C (ratios that denote stability) increased, whereas, hydrophilicity, yield of biochar, O/C, and H/C decreased. Discriminant analysis of data from 533 published datasets revealed that biochar derived from hardwood (HBC) and softwood generally have greater surface area and carbon content, but lower content of oxygen and mineral constituents, than manure- (MBC) and grass-derived biochars (GBC). GBC and MBC have abundant oxygen-containing functional groups than SBC and HBC. The sequence of stability and aromaticity of feedstocks was MBC < GBC < SBC < HBC. Therefore, SBC and HBC are suitable for sorption of hydrophobic molecules. Biochars produced from low HTT are suitable for

* Corresponding author at: Level-1, Advance Technology Centre (ATC-147), Ring Road, University of Newcastle, Callaghan Campus, NSW 2308, Australia.
E-mail addresses: Masud.Hassan@uon.edu.au (M. Hassan), Yanju.liu@newcastle.edu.au (Y. Liu), Ravi.naidu@newcastle.edu.au (R. Naidu), sjparikh@ucdavis.edu (S.J. Parikh), Jianhua.du@newcastle.edu.au (J. Du), Fangjie.qi@newcastle.edu.au (F. Qi), ian.willett@unimelb.edu.au (I.R. Willett).

https://doi.org/10.1016/j.scitotenv.2020.140714

removal of ionic contaminants, whereas those produced at high HTT are suitable for removal of organic contaminants. The influences of biochar properties on sorption performance of heavy metals and organic contaminants are critically reviewed.

Contents

1. Introduction

Biochars are frequently used as biosorbents for remediation of organic and inorganic molecules due to their multifunctional properties, the abundance of active sorption sites, stability, renewability, pollutant removal efficacy, availability, and low environmental impact (Beesley et al., 2011; Mohanty et al., 2018; Reyhanitabar et al., 2020; Singh et al., 2020; Wang et al., 2019a). Biochars are persistent black carbonaceous materials derived from the thermal conversion (e.g., pyrolysis, gasification) of raw feedstock materials that are readily biodegradable and consequently unsuitable as adsorbents (Abiven et al., 2014; Lehmann, 2007; Lehmann et al., 2006; Lehmann and Joseph, 2015; Lehmann and Kleber, 2015; Mohanty et al., 2018; Singh et al., 2020). Biochars contain an abundance of active adsorption sites, including C–C, *C*═*C*, OH—, metal—O/OH, CHO—, COOH, aromatic carbon skeletons, mineral crystal phases, and other oxygen-containing functional groups, rendering biochars as multifunctional adsorbents (Lehmann, 2007; Lehmann and Joseph, 2015; Liu et al., 2015; Wang et al., 2019a; Wang et al., 2020a; Zhang et al., 2020b).

Pyrolysis temperature and feedstock sources are the dominant factors influencing the physiochemical properties of biochars, including surface area, functional groups, hydrophobicity, stability, zeta potential, and pH (Ahmad et al., 2014; Budai et al., 2014; Chen et al., 2008; Pariyar et al., 2020; Weber and Quicker, 2018; Xiao et al., 2018). Optimization of pyrolysis temperature over the range of 200–800 °C has been used to control the properties of biochars, depending on the types of feedstocks materials and expected biochar properties. With increasing pyrolysis temperature, the carbon content, aromaticity, pH, ash content, surface area, stability, and pore size increase, while biochar yield, hydrogen content, oxygen content, H/C, and O/C ratios decrease (Downie et al., 2012; Mukome et al., 2013; Weber and Quicker, 2018).

An extensive range of biomass materials has been reported to serve as feedstock materials for producing biochars for environmental remediation (Angin, 2013; Chen et al., 2008; Chen et al., 2012a; Chen et al., 2015; Gai et al., 2014; Jung et al., 2016; Karunanithi et al., 2017; Uchimiya et al., 2011; Wang et al., 2020b; Weber and Quicker, 2018). Additionally, different types of feedstocks respond heterogeneously to particular pyrolysis conditions due to variations of cellulose $(C_5H_8O_4)_m$, hemicelluloses $(C_5H_8O_4)$, lignin $[C_9H_{10}O_3(OCH_3)_{0.9-1.7}]_n$ and inorganic mineral contents (Clemente et al., 2018; Dai et al., 2014; McBeath et al., 2014). Thus, biochars with distinctive physicochemical properties have been developed by pyrolyzing a wide range of feedstocks at the same temperature (Liu et al., 2015; Zhang et al., 2020a; Zhao et al., 2013). Consequently, it is challenging to select suitable feedstock materials and pyrolysis conditions for the synthesis of biochars for specific intended purposes. Furthermore, the properties of biochars and their sorption performance for organic and inorganic contaminants are quite unpredictable (Clemente et al., 2018; Dai et al., 2014).

The effects of pyrolysis conditions on the physical and chemical properties of biochars derived from particular types of biomass have been reported (Cantrell et al., 2012; Downie et al., 2012; Elkhalifa et al., 2019; Kan et al., 2016; Kloss et al., 2012; Mukome et al., 2013; Ronsse et al., 2013; Tag et al., 2016; Tripathi et al., 2016; Uchimiya et al., 2011; Weber and Quicker, 2018). Lian and Xing identified that the selection of feedstock materials and pyrolysis conditions are crucial in determining the physicochemical properties of biochars, but the effects of these variables are yet to be fully elucidated (Lian and Xing, 2017). However, quantitative analysis for understanding trends of physicochemical properties of biochar for agricultural purposes was initiated by Mukome and colleagues (Mukome et al., 2013). Xiao et al. developed “smart” biochar design for environmental applications (Xiao et al., 2018).

Despite considerable research and reviews on biochar (Lian and Xing, 2017; Petrov et al., 2017) there is still a lack of transparent and consistent information on the interrelationships between the physicochemical properties of biochar and their sources of feedstock biomass. Biochar properties, including surface morphology, stability, productivity, and active sites, are influenced by variations of structural cellulose, hemicellulose, lignin, and elemental composition (C, H, O, N, S, Si, K, and alkali metals) of feedstocks are not fully understood. In particular, there is inadequate information on how pyrolysis temperature and feedstocks influence the sorption properties of biochars.

We present a meta-analysis based on 533 datasets covering all major feedstocks types to understand the physicochemical properties of biochars produced over a wide range of pyrolysis temperatures (200–800 °C), and to elucidate quantitative interrelationships between feedstock types and pyrolysis temperature. The principal objective of the study is to determine reliable interrelationships between feedstocks, HTT, and biochar properties to assist end-users of biochars with decision making. We also review the effects of pyrolysis temperature on biochar sorption performance and mechanisms of their interactions with organic and inorganic contaminants. Furthermore, the effects of pyrolysis temperature on bulk composition (C, H, O), structural degradation, development of active sites, and surface morphology of biochars are critically evaluated. Our findings provide a fundamental understanding of the selection of raw feedstock materials and pyrolysis temperature for preparing biochars with desired properties as sorbents, and to facilitate future research.

2. Methodology

2.1. Data collection and synthesis

The meta-analysis was based on 533 dataset collected from peer-reviewed articles on the effects of pyrolysis on the physicochemical properties of biochar produced from major types of feedstock. About 86, 130, 102, and 215 datasets were collected for manure, hardwood, softwood, and grass derived biochars, respectively. Manure waste was considered to be primarily animal feces (Gollehon et al., 2001). Hardwood was considered to be angiosperm and dicotyledonous deciduous trees, whereas softwood was considered to be evergreen gymnosperm trees such as conifers (Butterfield, 2006; Parham and Gray, 1984; Wiedenhoeft, 2010). Grasses were considered to be vegetation of the *Poaceace* and *Gramineae* families (Tzvelev, 1989). All datasets were collected from the peer-reviewed journal database, and UC Davis biochar database (biochar.ucdavis.edu) (Supplementary File 2). The articles that reported biochar produced by slow pyrolysis, reported synthesis details of biochar, and adequately characterized biochars, were selected. The datasets with more likely similar analytical and characterization methods were collected to permit statistical analysis and derivation of general conclusions. Pertinent data were derived for feedstock types, including elemental composition, O/C, H/C, stability (O/C vs. H/C), biochar yield, ash production, and pH. Such data were available because of their importance for biochars functioning as sorbents (Downie et al., 2012; Mukome et al., 2013; Weber and Quicker, 2018). O/C and H/C data were calculated from the raw C, H, O data to avoid inconsistency.

2.2. Statistical strategy and assessment

To establish interrelationships between feedstock sources of biochars, their physiochemical properties, and HTT conditions, the Pearson product-moment correlation coefficient and correlation matrix were utilized for cross pairs of biochar properties to identify the strength and direction of association among the variables. Significant relationships were determined at the 95% confidence interval. Adjusted coefficients of determination ($0 \le \text{Adj } r^2 \ge 1$) were also included for each paired correlation of the properties of biochars. Box–plots were used for quantifying the distribution of each parameter, which were placed diagonally into the correlation matrix. Rectangular boxes indicated interquartile ranges (Q 1(25 percentile) to Q 3 (75 percentile)), where the vertical line of the boxes indicates the median value. The standard deviation of each variable was also outlined in the box-plots. Radar plots, scatter plots, and line plots were also drawn to find interrelationships between sorption parameters and performance.

2.3. Limitations of the study

Each correlation matrix provides an abundance of information to help understand the interrelationships of all the physicochemical properties of biochars. A limitation of this study is the potential variation within each feedstock type (e.g., manures), which could be dissimilar based on the geographical location, nutrition sources, and other ex-situ conditions (Cantrell et al., 2012; Morales et al., 2015). For example, Cabtrell et al. used different sources of manures, including turkey, poultry litter, feedlot, swine, and dairy, and the properties of each type of biochar were similar, except for those derived from swine manure (Cantrell et al., 2012). Therefore, we note potential unresolved bias due to the lack of detailed information in some of the literature, which could be considered in future research work. Additionally, comparisons of the sorption performance of biochars from the range of feedstock types are quite challenging due to variations of equipment, experimental conditions, and insufficient data from homogeneous systems. Therefore, we only considered relevant research articles to describe the influence of pyrolysis temperature on sorption parameters.

3. Review on pyrolysis of feedstocks and the properties of biochars

3.1. Degradation and transformation of cellulose, hemicellulose, and lignin

Raw feedstocks are mainly composed of 20–60% cellulose $(C_5H_8O_4)_m$, 15–60% hemicelluloses ($C_5H_8O_4$), and 5–40% lignin $[C_9H_{10}O_3\ (OCH_3)_{0.9-1.7}]_n$, depending on the source materials (Fig. S1). Cellulose and hemicellulose contribute to the development of oxygen-containing functional groups and aromatic rings in biochars during pyrolysis (Lian and Xing, 2017; Liu et al., 2017; Yang et al., 2007a). Hemicellulose and cellulose are fragmented and transform faster than lignin. Cellulose is primarily depolymerized into oligosaccharides and develop glucosidic bonds to produce D-glucopyranose and levoglucosan. Levoglucosan dehydrates to levoglucosenone, which then goes through several processes including decarboxylation, dehydration, aromatization, and condensation to form biochars (Qu et al., 2011; Shen and Gu, 2009; Yang et al., 2007a; Zhang et al., 2019). The mechanism of hemicellulose degradation is more likely similiar to cellulose degradation. However, lignin decomposition is quite complex compared to cellulose and hemicellulose decomposition (George et al., 2014; Liu et al., 2015). A free radical reaction is the most critical mechanism for lignin degradation. The breaking of β-O-4 lignin linkages generates free radicals that can initiate a free radical chain reaction (Liu et al., 2015; Qu et al., 2011; Yang et al., 2007a). These free radicals can capture other species (e.g., C_6H_5-COOH) and form decomposition products such as vanillin and 2-methoxy-4-methylphenol (Liu et al., 2015; Peters, 2011). These processes can lead to chain propagation of aliphatic carbon compounds. The reaction terminates when two radicals collide and form a more stable carbon compound through random repolymerisation. However, the pathways of free radical formation and collision are complex. A complete understanding of the pyrolysis of lignin remains unknown. The cellulose, hemicellulose, and lignin decomposition during pyrolysis were described in depth by Liu et al. (Liu et al., 2015).

A large proportion of cellulose and hemicellulose in feedstocks can produce a wide range of oxygen-containing functional groups, but small biochar yields. Alternatively, a greater proportion of lignin leads to higher biochar yield due to the high fixed carbon and thermal

stability of aromatic monomers than the aliphatic carbon phases of cellulose and hemicellulose. However, with increasing HTT there are fewer polar functional groups and more non-polar functional groups due to losses of hydroxyl and aliphatic groups (Chen et al., 2008; Chen et al., 2012a; Keiluweit et al., 2010; Qu et al., 2011; Uchimiya et al., 2011; Uchimiya et al., 2010b).

3.2. Pyrolysis temperature and development of surface functional groups

Differences in content and intensity of functional groups depend on feedstock sources, medium of pyrolysis, and HTT (Fig. S3). In particular, pyrolysis temperature is critical for tailoring desired functional groups. The most common functional groups of biochars include C—– –O—– –, C—– –C, C═C-, OH-, CH-, Metal-O-, CHO-, COO-, and carbon skeleton (Fig. S2 & S3), that are developed on biochar surfaces by oxidation, dehydration, and decarbonization processes. However, biochars produced by pyrolysis under 100% nitrogen atmospheres have higher contents of oxygen-containing functional groups than those produced under air (Luo et al., 2015).

Hypothetically, the pyrolysis of feedstock materials can be divided into three stages. A wide range of functional groups transform from one state to another depending on the HTT and duration of pyrolysis. For example, in the first stage (< 200–300 °C), the feedstocks start to break down, and in the second stage (300–600 °C), a wide range of aliphatic functional groups derived from cellulose and hemicellulose start to form (Lian and Xing, 2017; Liu et al., 2015). At 300–350 °C, the cellulose and hemicellulose start to degrade and form symmetric C—– –O stretching (1110 cm^{-1}), aromatic C═C stretching (1475–1600 cm^{-1}), C—– –H stretching (855 cm^{-1}), CH_2 and CH_3 alkanes bend (1375 and 1465 cm^{-1}), C═O stretching of conjugated ketones (1600 cm^{-1}), OH bending of alcohol (3300–3400 cm^{-1}), and O—– –H bonding of phenol (1375 cm^{-1}) (Cantrell et al., 2012; Cao et al., 2010; Lian and Xing, 2017; Liu et al., 2015). In the third stage (600–900 °C), benzene derivatives (700 cm^{-1}), and polycyclic structures start to form through transformations (Lian and Xing, 2017; Yang et al., 2007b). With increasing pyrolysis temperatures, oxygen-containing functional groups gradually decreased (Chen and Chen, 2009; Chen et al., 2008; Chen et al., 2012a; Fang et al., 2013; Keiluweit et al., 2010). Above 600–800 °C, most of the prominent spectral features noted at lower temperatures were lost, and the FTIR spectra resembled an ordered graphitic structure (Lian and Xing, 2017). Aliphatic structures, including C═O, carboxyl, ketone, and esters, are completely degraded at high temperatures (Cantrell et al., 2012; Cao et al., 2010; Chen et al., 2008; Lian and Xing, 2017). Therefore, biochars produced at low temperatures are mostly hydrophilic due to the presence of a wide range of oxygen-containing functional groups (Lian and Xing, 2017). Conversely, biochars derived at high temperatures are more likely to contain aromatic structures and skeletons (Keiluweit et al., 2010; Kloss et al., 2012; Sharma et al., 2004). Aromatic rings of biochar result in hydrophobic functional groups (Lian and Xing, 2017). Thus, aromatic structures are predominantly produced at higher HTT, whereas oxygen-containing functional groups are prominent at lower HTT (Chen et al., 2008; Pignatello et al., 2017).

3.3. Effect of HTT on the surface morphology of biochars

Scanning Electron Microscope (SEM) micrographs of biochars produced from sawdust at different pyrolysis temperatures (200–600 °C) are highlighted in Fig. 1. A definite change in the SEM images was observed with increasing pyrolysis temperature (Fig. 1a-1f). The SEM micrograph of sawdust pyrolyzed at 200 °C (Fig. 1b) did not show any visible pores, whereas at 600 °C (Fig. 1f) biochar displayed honeycomb-like pores of a carbonaceous skeleton derived from lignocellulose. With increasing temperature the biomass surface started to decompose and volatilize. The morphology of biochar at 300 and 400 °C exhibited several visible pore structures (Fig. 1c & d). Pyrolysis at 500 °C showed that portions of the skeletal structure appeared to be due to the decomposition of cellulose and hemicellulose (Fig. 1e). More fractured structures appeared at 600 °C and it appeared that biochar had melted and coalesced into a mass of vesicles (Fig. 1f).

Transmission electron microscope (TEM) images (×800 K) of biochar highlighted detailed surface morphology of biochar derived from sugarcane bagasse (Fig. 1g–k). The TEM image of raw biomass showed an amorphous structure. However, at mild pyrolysis temperatures (250–350 °C), the amorphous carbon started to reorganize due to the breakdown of cellulose and hemicellulose structures. At high pyrolysis temperature (600 °C) the biochar surface organized into a regular crystalline structure that was most probably graphite. Generally, graphitic carbon phases and porous structures of biochar enhance sorption of organic contaminants through hydrophobic interactions and intra-particle diffusion, but reduce sorption of inorganic contaminants due to reductions of oxygen-containing functional groups (Chen et al., 2008; Gai et al., 2014; Hassan et al., 2019; Xiao et al., 2018).

4. Results and discussions of the meta-analysis

4.1. Bulk composition (C, H, O), and mineral constituents of biochars

C, H, and O are the major elemental components of feedstock sources. The elemental content of feedstocks vary with biomass type (Fig. S4) (Xiao et al., 2018). Carbon is the key element for biochar yield and the development of functional groups (Weber and Quicker, 2018). The H and O contents of feedstocks also strongly influence biochar properties, including polarity and association/dissociation of hydrogen ions, which can influence biochar interactions with organic and inorganic solutes (Chen et al., 2014b; Qian and Chen, 2013; Spokas, 2010; Xiao et al., 2018; Xiao et al., 2016). The effects of pyrolysis temperature (200 °C–1000 °C) on the C, O, H, and N contents of biochars derived from a variety of feedstocks (GBC, HBC, SBC, MBC) are illustrated in Fig. 2. Differences in the C, N, H, and O contents are distinguishable between the various feedstock sources. The trend for carbon content was: HBC > SBC > GBC > MBC, whereas the trend for oxygen content was reversed: MBC > GBC > SBC > HBC (Fig. 2). This indicates that MBC and GBC produce abundant oxygen-containing functional groups, whereas wood-derived biochar (HBC and SBC) had high degrees of aromatic structure. However, the total nitrogen content of biochar remained almost the same as corresponding raw feedstocks materials (Hassan et al., 2019). At high pyrolysis temperatures, low CEC, high pH and high point of zero net charge of biochars was observed, whereas at low pyrolysis temperatures, high CEC, low pH and low point of zero net charge can be attributed to the presence of oxygen-containing acidic functional groups, including carboxylic and phenolic groups (Banik et al., 2018; Menéndez et al., 1995).

Inorganic elements are also present in biochars and their concentrations vary depending on the source of feedstock and pyrolysis conditions. Mineral constituents generally comprise <5 g/kg of biochars (Fig. 3). Biochar functionality as sorbents is not only influenced by C, H, and O, but also by inorganic elements present in the precursors, which varies depending on the feedstock types. Mineral elements can also influence biochar pH, morphology, active sites, and degradation pathways. The functions and roles of mineral constituents of biochars were studied in detail by Xiao et al. (Xiao et al., 2018). Usually, manure-derived biochars have more inorganic constituents than grass and soft- or hard-wood derived biochars, which increases with increasing HTT (Fig. 3a). The effects of pyrolysis temperature on the variation of elemental composition of different feedstock materials are highlighted in Fig. 3b. With increasing pyrolysis temperature the relative weight % of inorganic elements (except those that are volatile, e.g., N) increased due to evaporation and reductions of hydrogen and oxygen contents from raw biomass, but their content by weight remained almost the same. Recently, Sørmo et al. observed in highly pyrolyzed (800 °C) biochar derived from waste timber that the content of heavy metal(loid)s

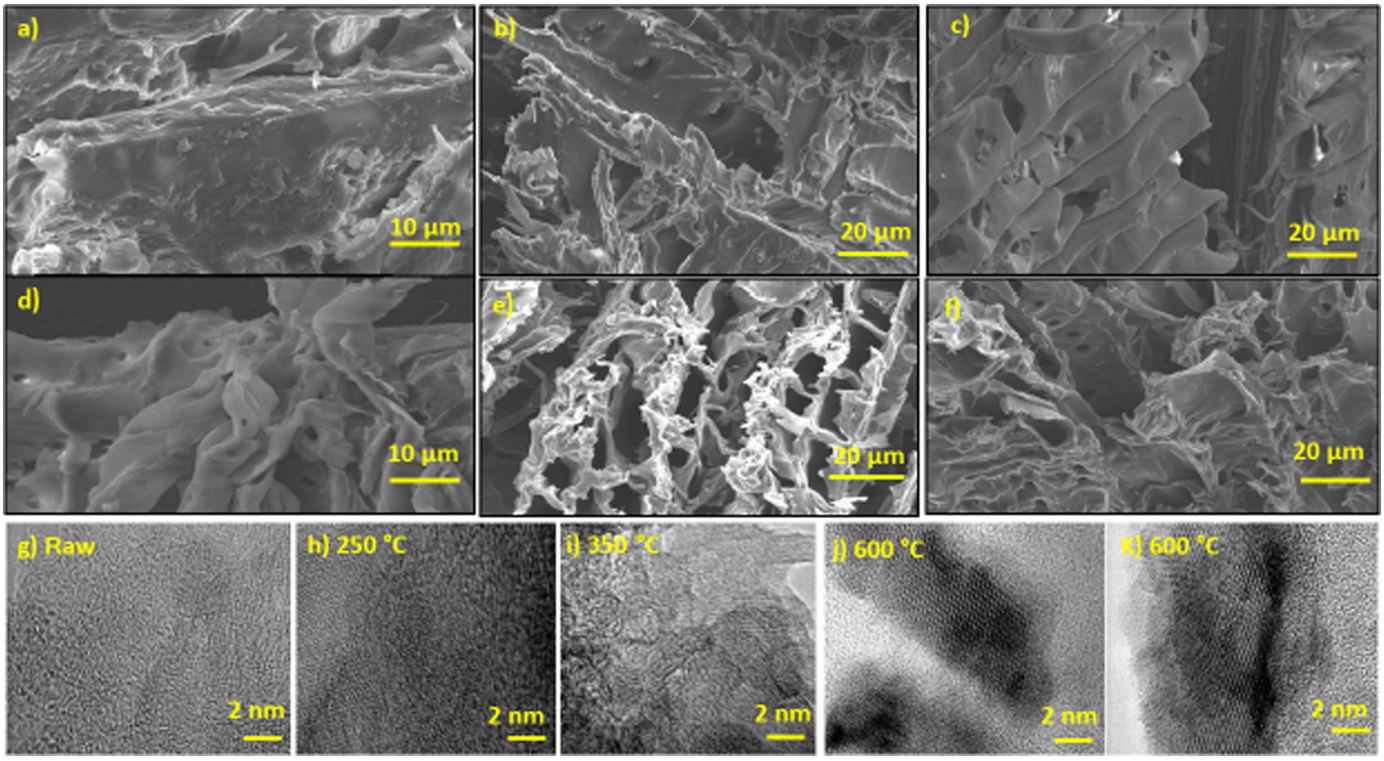

Fig. 1. Scanning electron microscopy (SEM) micrographs of biochars derived from sawdust biomass at different HTT: a) raw condition; b) 200 °C; c) 300 °C; d) 400 °C; e)500 °C; f) 600 °C (Liu et al., 2016); TEM image (x800 K) of g) raw sugarcane bagasse (SB) and SB derived biochars pyrolysed at h) 250 °C, i) 350 °C, j) & k) 600 °C.

(Cu, Cr, Pb, Zn, As) was reduced during pyrolysis resulting in metal emissions (Sørmo et al., 2020).

Inorganic constituents of biochars can improve their stability against thermal degradation and participate in the adsorption of contaminants. For example, pyrolysis of silicon-rich feedstocks, including sugarcane bagasse, rice straw, and wheat straw, can convert amorphous silicon into silicic acid and crystalline SiO_2 at low (< 250 °C) and high (> 500 °C) HTT, respectively (Liu et al., 2013a; Wang et al., 2019b;

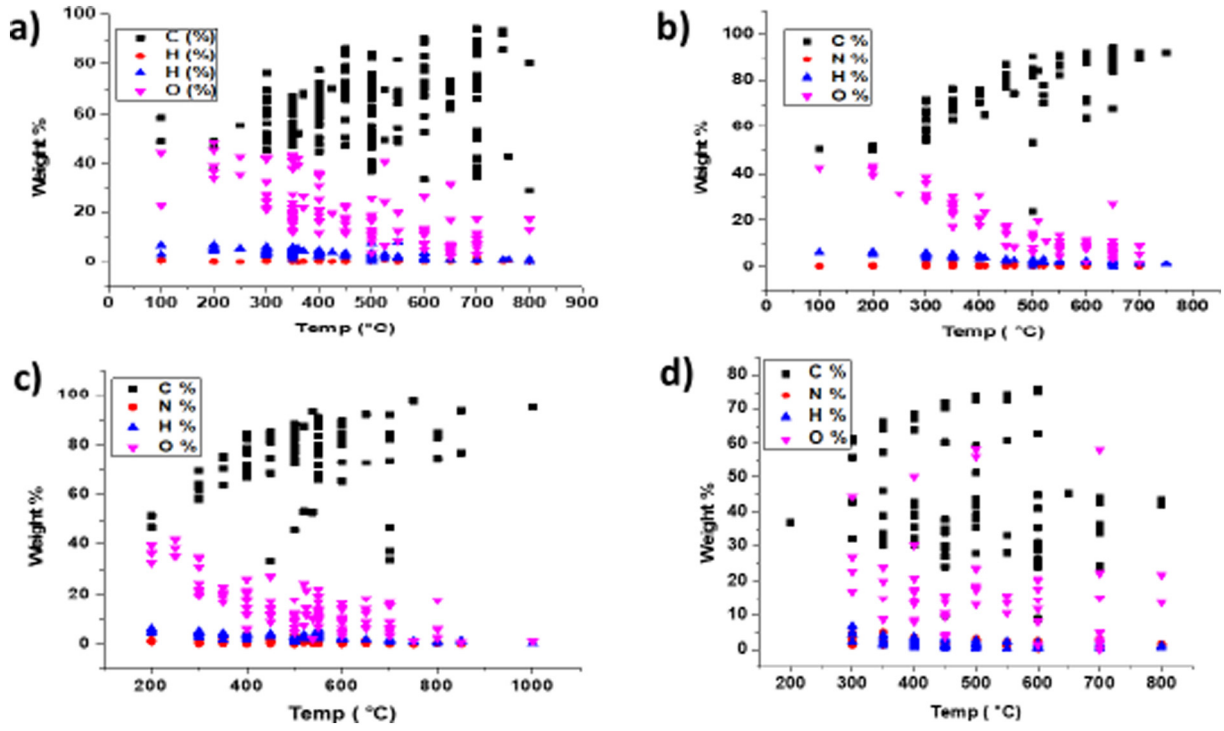

Fig. 2. Effects of pyrolysis temperature on the elemental composition (C, H, O, & N) a) grass-derived biochar (GBC) b) softwood -derived biochar (Ahmady-Asbchin and Bahrami) c) hardwood -derived biochar (HBC) d) manures -derived biochar (MBC) (Data sources attached as Supplementary File).

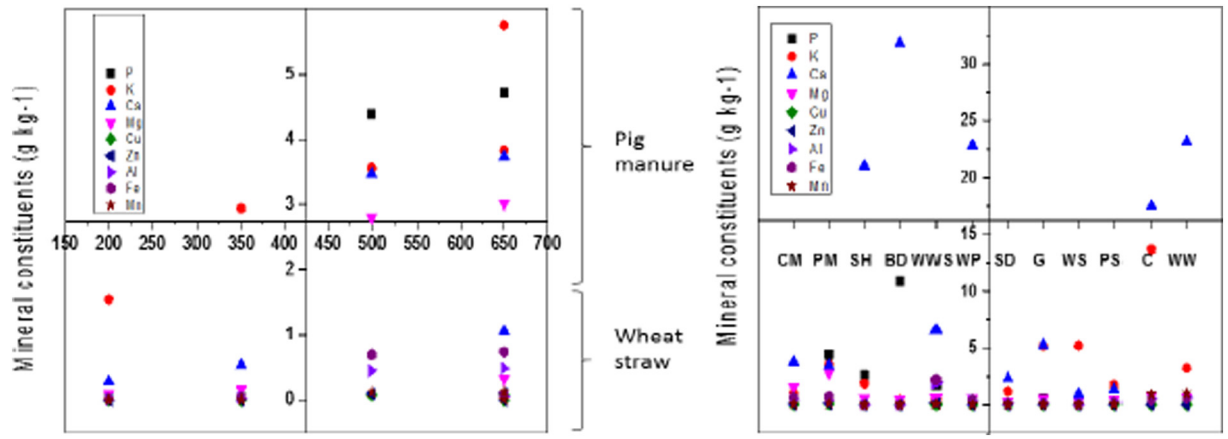

Fig. 3. a) Effects of pyrolysis temperature (200–650 °C) on the mineral constituents (g/kg^{-1}) of pig manure- and wheat straw- derived biochar, b) Mineral constituents (g/kg^{-1}) of cow manure (CW), pig manure (PM), shrimp hull (SH), bone dregs (BD), wastewater sludge (WWS), waste paper (WP), sawdust (SD), grass (G), wheat straw (WS), peanut shell (PS), chlorella (C), and water weeds (WW) derived biochar pyrolysis at 500 °C (Data extracted from Zhao et al. (Zhao et al., 2013)).

Xiao et al., 2014). Silicon is a major inorganic phase involved in metal co-precipitation. Silicon can also protect organic phases against thermal decomposition during pyrolysis (Wang et al., 2019b). Therefore the silicon within biochars acts as a co-precipitator of adsorbed heavy metal (loid)s (Cao et al., 2009; Chen et al., 2008; Guo and Chen, 2014). Fe and Ni species in biochar were shown to increase the sorption of anions and the catalytic degradation rate of organic contaminants (Shen et al., 2014; Wan et al., 2020; Wu et al., 2020; Yan et al., 2015). Abundant Fe species and engineered species (Fe_2O_3, Fe_3O_4, FeO, Fe_3C, FeOH, Fe-metal, and other metal complexes of iron) in feedstocks can induce ferromagnetism in biochar resulting in easy separation and recovery after sorption (Shen et al., 2014; Wan et al., 2020; Wu et al., 2020; Xiao et al., 2018; Yan et al., 2015). Fe-containing functional groups improve anion sorption capacity, promote carbonization, and perform as catalysts for the degradation of non-persistent organic contaminants (Shen et al., 2014; Wang et al., 2016; Yan et al., 2015). Similarly, Mg and Mn containing biochars (Mg/Mn-O/OH, Mg/Mn-CO_3, Mg/Mn-metal complex) also contribute to the removal of ionic contaminants by introducing cation exchange and electrostatic interaction through metal-O/OH functional groups, depending on the pH of the sorption

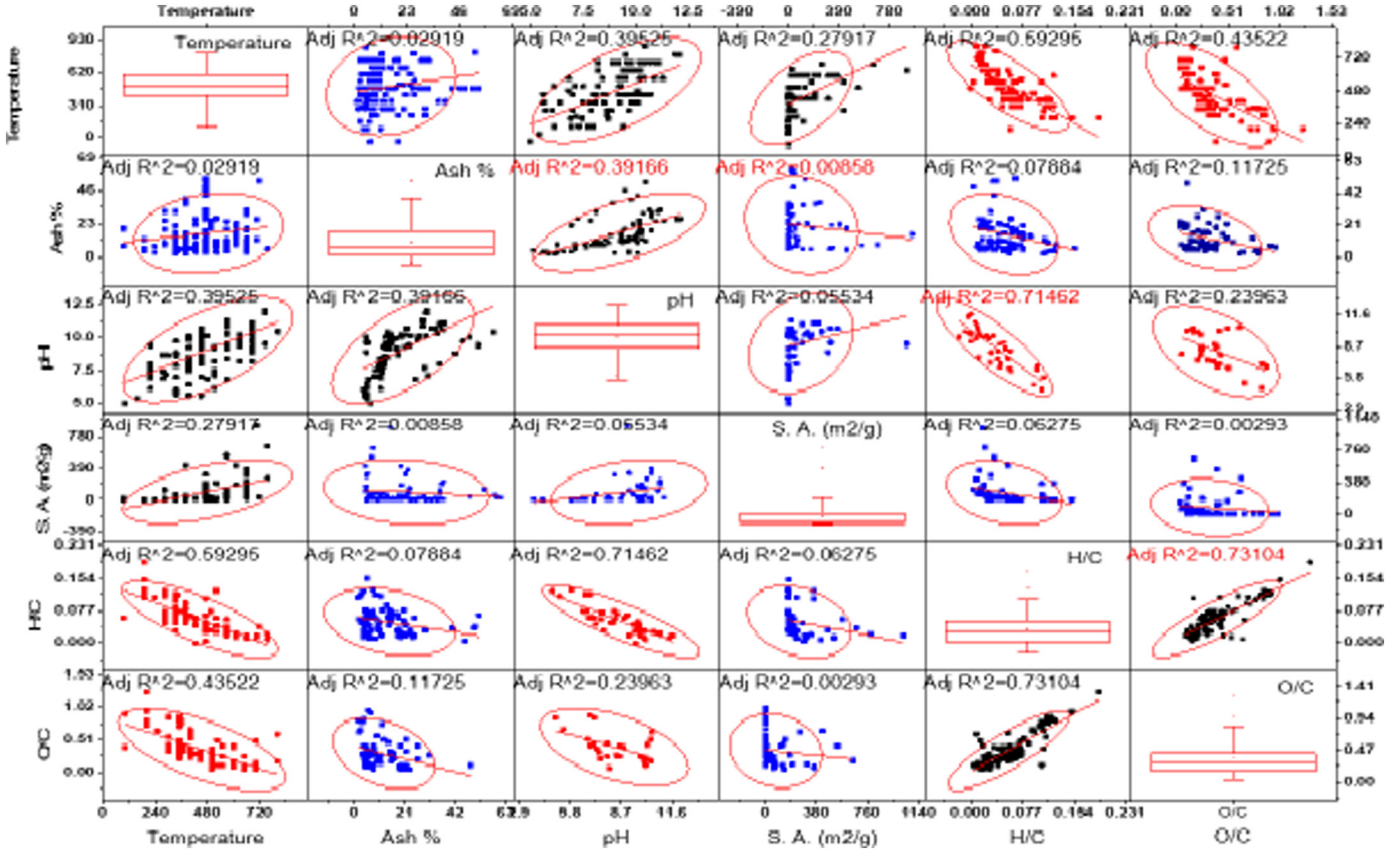

Fig. 4. Pyrolysis effects on the physicochemical properties of grass-derived biochar (GBC) and their interrelationships with bivariate pair scatterplots (95% confidence level) with trend lines.

medium (Liu et al., 2013b; Wang et al., 2015b; Xiao et al., 2018; Zhang et al., 2012). Metal phases of biochar can also precipitate heavy metal (loid)s, degrade organic contaminants, and enhance syngas production. Metals can also act as catalysts or activators in biochar (Liu et al., 2013b; Shen et al., 2014; Wang et al., 2015b; Yan et al., 2015; Zhang et al., 2012). The presence of P and N in biochar can improve thermal stability and precipitate heavy metal(loid)s (Cao et al., 2009; Rondon et al., 2007). Nitrogen-containing species (imine-N, amine-N, acylamide-N, pyridine, NH_4^+, NO_3^-, NO_2^-) improve the stability and reactivity of biochars (Rondon et al., 2007; Wang et al., 2016). Phosphorus species, including monophosphate ester, phosphate di-ester, PO_4^{3-}, and $P_2O_7^{4-}$, can contribute to the precipitation of heavy metal(loid)s, in a similar way to N and S species (Xiao et al., 2018).

During pyrolysis, K, Cl, Ca, and Mg form complex molecules with organics or volatilize at high temperatures. P, S, N can also volatilize at low temperatures (Liu et al., 2015; Xiao et al., 2018). Some alkali metals have catalytic characteristics that lead to the production of gaseous compounds and cracking of biochars structure resulting high surface area and porosity. Mineral phases of biomass influence degradation, yield of biochar, and biochar properties (Collard et al., 2012; Di Blasi et al., 2009; Qu et al., 2011). For example, the mineral contents of feedstock sources positively correlated with CEC, pH, and ash production but were negatively correlated with carbon content, and consequently, biochar yield (Sun et al., 2016; Yuan et al., 2011). However, the extent and influences of the catalytic effects of minerals on biomass for the transformation of aliphatic carbon into aromatic and graphite phases during HTT require further study.

4.2. Effects of HTT on properties of Gramineae-derived biochar (GBC)

Different species of grasses, including crop residues, napier grass, wheat straw, cordgrass, giant reed, rice straw, silver grass, and sugarcane bagasse, are commonly used as feedstock materials for grass-derived biochar (GBC) (Chun et al., 2004; Crombie and Mašek, 2015; Harvey et al., 2011; Wang et al., 2013). The effects of pyrolysis temperatures on the physiochemical properties of GBC are significantly different from those of HBC and MBC due to considerable variation of chemical composition. The effects of pyrolysis temperature on the major physiochemical properties of GBC, including their interrelationships, are highlighted in Fig. 4. There is lack of information for the physiochemical properties of GBC generated below 200 °C and above 800 °C (Fig. 4). Grasses are pyrolyzed faster than hardwood and softwood feedstocks due to low thermal resistance. Large surface areas are generally obtained in biochars produced at high pyrolysis temperatures due to the volatilization of hydrogen and oxygen (Fig. 4). Both surface area and pore volume of biochars increase slightly and have positive correlations with increasing pyrolysis temperature, whereas the yield of biochars decreases, and consequently, ash production increases. GBC generally produces large amounts of ash due to the presence of alkali metals, which is similar to MBC. The pH of GBC increased with HTT and ranged from 5 to 11 due to increases in hydroxyl, carboxyl, and carbonyl groups, and the presence of alkali metal hydroxides in the feedstocks.

The ratios O/C and H/C indicate the polarity and aromaticity of biochars, which are critical properties for applications of biochar as adsorbents (Crombie et al., 2013; Leng et al., 2019). High aromaticity is suitable for sorption of organic contaminants. The H/C molar ratio is used to estimate the carbonization of biosorbents. A decreasing H/C molar ratio suggests a higher degree of carbonization and smaller amounts of plant residues (e.g., cellulose, hemicellulose) (Samsuri et al., 2013). The O/C molar ratio can be used to indicate the hydrophilic nature of biochars, which vary according to biomass type and pyrolysis temperature (Mukome et al., 2013; Uchimiya et al., 2011). Decreasing trends of O/C ratio with increasing temperature indicate decreasing polarity of biochar, and oxygen-containing

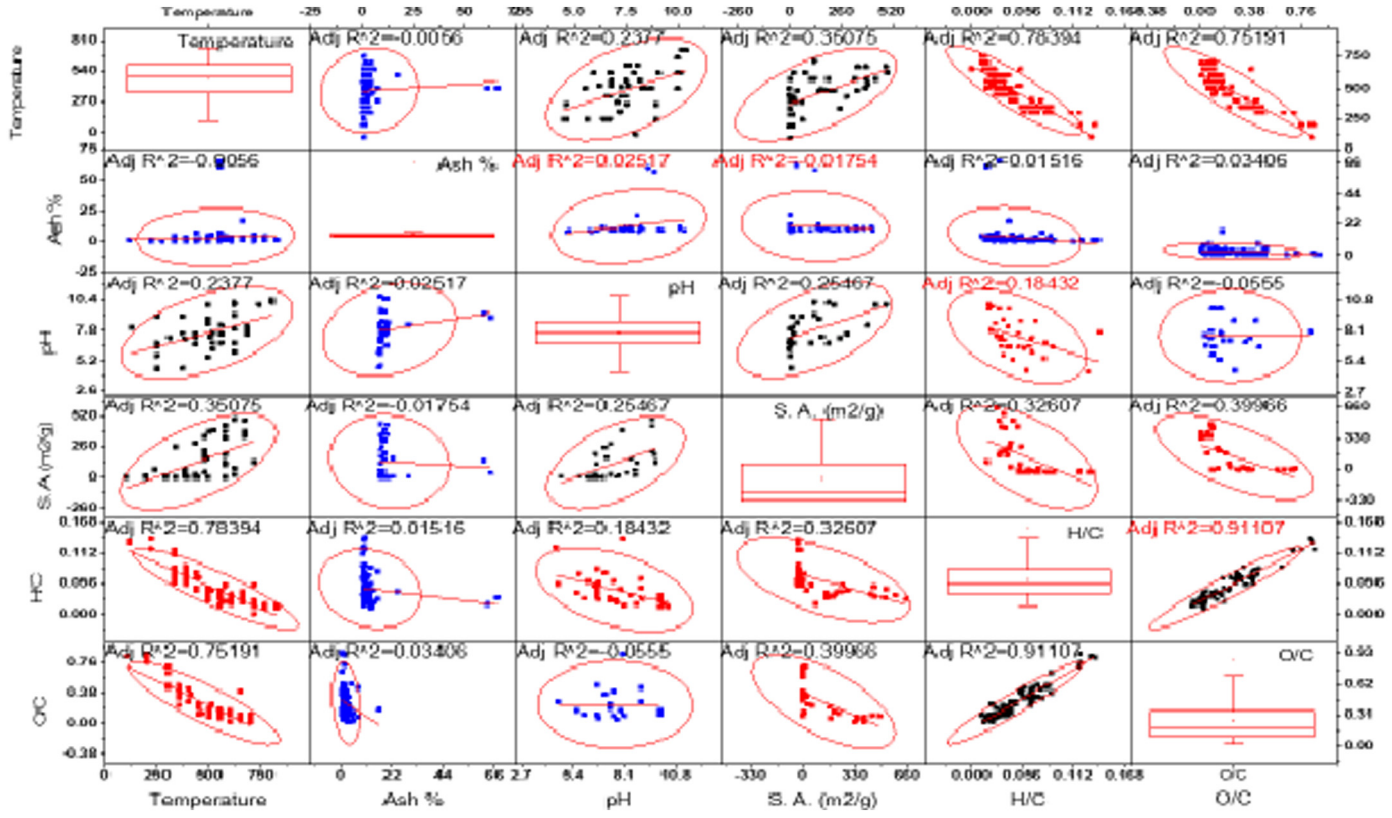

Fig. 5. Pyrolysis effect on the physicochemical properties of softwood-derived biochars (SBC) and their interrelations, with bivariate pair scatterplots (95% confidence level) with a trend line.

functional groups. Ratios of O/C and H/C below 0.4 are preferred to ensure biochar stability (Cantrell et al., 2012; Leng et al., 2018). Oxygen loss from biochars was inversely proportional to aromaticity, and ash content (Han et al., 2018). With increases in pyrolysis temperatures the molar ratios of H/C and O/C increased due to the greater degree of carbonization (Chen et al., 2008; Keiluweit et al., 2010). GBC showed higher polarity and functionality than other types of feedstock materials due to its greater O/C values. In the meta-analysis, positive correlations were shown for HTT versus pH ($r^2 = +0.40$), HTT versus surface area (SA) ($r^2 = +0.28$), pH versus ash content ($r^2 = +0.39$) and H/C versus O/C ($r^2 = +0.73$). Negative correlations were found for HTT versus O/C ($r^2 = -0.43$), H/C versus HTT ($r^2 = -0.59$), and pH versus H/C ($r^2 = -0.71$). The ranges of major physicochemical properties, with standard deviations, for GBC are shown diagonally by using box plots with the scatter matrix (Fig. 4).

4.3. Effects of HTT on properties of softwood-derived biochar

The most commonly used softwoods for biochar synthesis are pine, redwood, willow, hemlock, and alder. Various physiochemical properties of SBC and their interrelationships are depicted in Fig. 5. The distribution of physicochemical properties, with standard deviations, of SBC are also represented with box-plots (Fig. 5). The surface area of softwood-derived biochar can reach 500 m^2/g, which is much larger than that for GBC and MBC, but smaller than that for HBC. The pH of SBC ranged from 4 to 10 for pyrolysis temperatures of 200–800 °C (Fig. 5). There was an increasing trend in pH of SBC with increasing pyrolysis temperature (Fig. 5). With increases in temperature, C—–C, C═C, C═O, and C═H bonds break down and start to form O—–H, CHO-, COOH-, and benzene rings, and their polymers that contain more –OH functional groups and hence further raise the pH of SBC. The aromaticity increased proportionally to carbon content but inversely with O content (Wiedemeier et al., 2015). Surface hydrophilicity of softwood biochar increased with pyrolysis temperatures. Wood-derived biochars (SBC and HBC) have small H/C vs. O/C values that indicate high stability and aromaticity (Abiven et al., 2014; Weber and Quicker, 2018). The ash production from softwood is much smaller (below 5%) than that derived from GBC and MBC. Softwood-derived biochar is more stable than GBC and MBC, but less stable than HBC. For SBC positive correlations were found for HTT versus pH ($r^2 = +0.24$), HTT vs. surface area ($r^2 = +0.35$), and H/C vs. O/C (+0.91). Negative correlations were found for HTT vs. O/C ($r^2 = -0.75$), H/C and HTT ($r^2 = -0.78$), pH vs. H/C ($r^2 = -0.18$).

4.4. Effects of HTT on properties of hardwood-derived biochars (HBC)

Eucalyptus, cottonwood, oak, mahogany, walnut, teak, birch, and beech are common hardwoods used for biochar production. Fig. 6 illustrates temperature effects on the physicochemical properties of HBC and their interrelationships. The distribution of significant physicochemical properties is also depicted diagonally by box-plots and standard deviations (Fig. 6). The surface area of HBC was much greater than that of GBC, MBC, or SBC. The surface area and pH increased with increasing HTT and decreased with increasing hydrogen and oxygen contents. The pH generally increased with HTT due to the transformation of aliphatic carbon structure into aromatic carboxylic and phenolic carbon (Lian and Xing, 2017). However, the ash contents were lower than those for GBC and MBC due to the small content of alkali metals in hardwood feedstocks, which is consistent with a previous study by Mukome and colleagues (Mukome et al., 2013). The ash content of HBC reached up to 20%, whereas for GBC and MBC it generally reached up to 40 and 70% ash, respectively (Figs. 4–7). Wood-derived biochars (SBC and HBC) show lower polarity but higher stability than any other type of feedstock material, making them suitable for sorption of organic contaminants (Chatterjee and Saito, 2015; Hassan et al.,

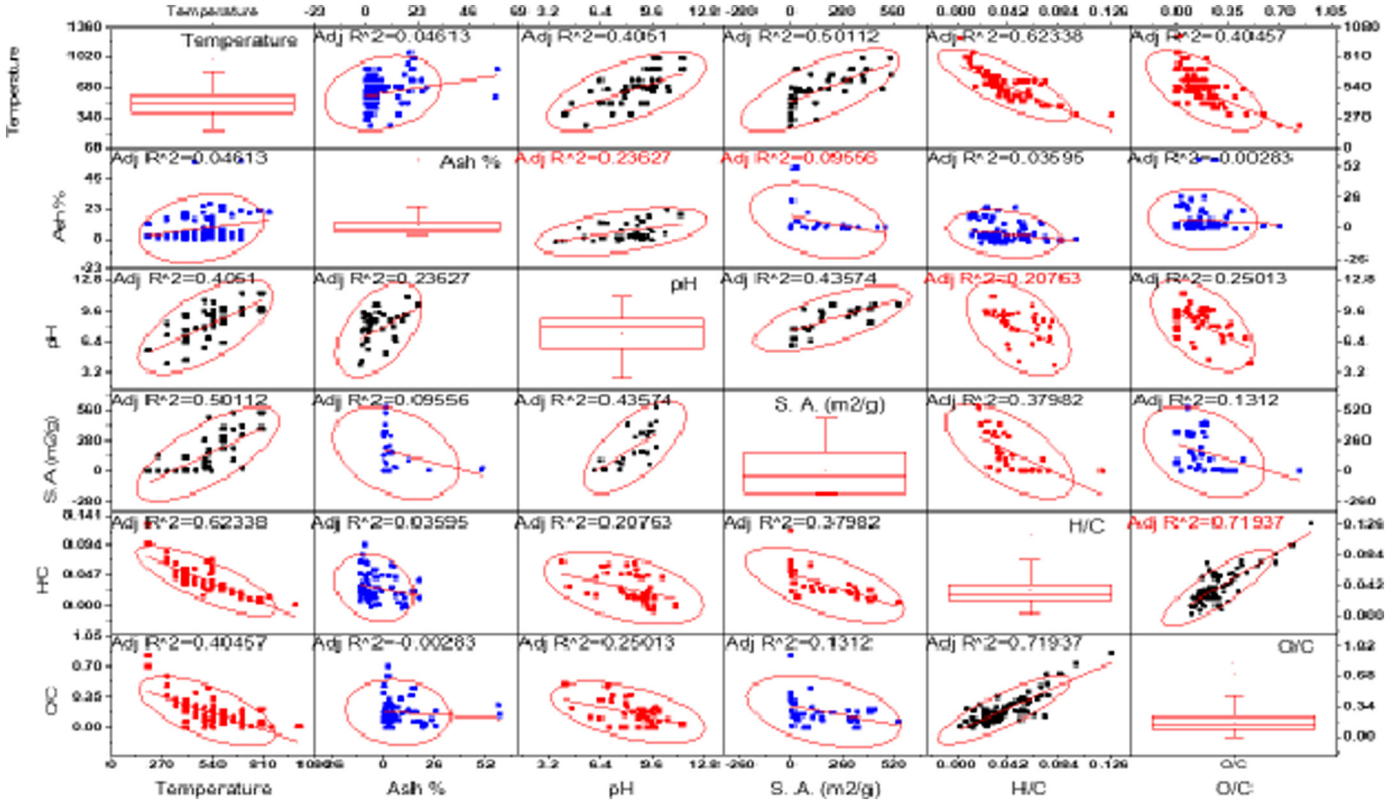

Fig. 6. Pyrolysis effects on the physicochemical properties of hardwood-derived biochar (HBC) and their interrelations, bivariate pair scatterplots with trend lines (95% confidence level).

2020; Yaashikaa et al., 2019). Positive correlations were found for HTT vs. pH ($r^2 = +0.41$), HTT vs. surface area ($r^2 = +0.50$), and H/C vs. O/C ($r^2 = +0.71$), whereas negative correlations were found for HTT vs. O/C ($r^2 = -0.40$), H/C and HTT ($r^2 = -0.62$), pH vs. H/C ($r^2 = -0.20$).

4.5. Effects of HTT on the properties of manure-derived biochar (MBC)

Poultry litter and manures from dairies, turkeys, and swine are used as feedstock materials for biochar preparation. Fig. 7 illustrates the effects of temperature on the physicochemical properties of manure-derived biochar (MBC) and their interrelationships. The distribution range of major physiochemical properties of biochar is highlighted diagonally by box-plots (Fig. 7). MBCs generally had smaller surface areas than GBC, SBC, and HBC, with pyrolysis temperatures up to 800 °C, and ranged from 5 to 80 m^2/g (Fig. 7). MBC had comparatively higher pH than those of HBC, SBC, and GBC. Manures contain more alkali and the alkaline metals than other biochars, and when oxidized at high temperatures form oxides (Hagemann et al., 2018), leading to high ash content. The ash content of manures was up to 70% with pyrolysis at 800 °C. The ash content was inversely proportional to biochar yield. Positive correlations were found between pH vs. HTT ($r^2 = +0.40$), and pH vs. ash percentage ($r^2 = +0.43$), whereas negative correlations were found for HTT vs. H/C ($r^2 = -0.54$), and pH vs. H/C ($r^2 = -0.42$).

4.6. Trends of physiochemical properties of biochars

In general, some reports stated that biochar carbon content, pH, ash content, surface area, and stability increase, while H/C and O/C decrease with increased HTT (Downie et al., 2012; Mukome et al., 2013; Weber and Quicker, 2018). However, our meta-analysis with wide ranges of feedstock materials and HTT showed that such relationships varied among individual types of feedstock. The degree of variation in the characteristics of biochar has been identified quantitatively, which was unknown previously. For example, the correlation coefficients of surface area vs. HTT were +0.28, +0.35, +0.50, and +0.05 for GBC, SBC, HBC and MBC, respectively (Table 1). There were moderately positive correlations between HTT and the surface areas of GBC, SBC, and HBC, but not with MBC. Similarly, MBC showed little correlation between HTT and O/C, while biochars derived from other feedstocks had moderate negative correlations with HTT (Table 1). Negative correlations were also observed between surface area vs. ash %; pH vs. H/C; O/C vs. ash%; pH vs. O/C; surface area vs. H/C; and surface area vs. O/C. On the other hand, positive correlations were found between ash % vs. pH; pH vs. surface area; and H/C vs. O/C (Table 1). The detailed interrelationships and degree of trends (+ ve and −ve) of correlation coefficients for individual parameters of each biochar (SBC, HBC, SBC, and MBC) are presented in Table 1. Interrelationships between properties of biochar with HTT are therefore specific for individual feedstock materials.

4.7. Effects of pyrolysis temperature on biochar functionality for removal of contaminants

The sorption by biochar of organic and inorganic contaminants, including heavy metal(loid)s, pharmaceuticals, antibiotics, agrochemicals, and other emerging contaminants can reduce the toxicity of such contaminants (de Andrade et al., 2018; Elimelech and Phillip, 2011; Montgomery and Elimelech, 2007; Oberoi et al., 2019; Patel et al., 2019; Rajaganapathy et al., 2011; Shannon et al., 2008). Feedstocks and pyrolysis temperatures for the synthesis of biochar can be selected to produce tailored adsorbent properties for the removal of specific types of contaminants.

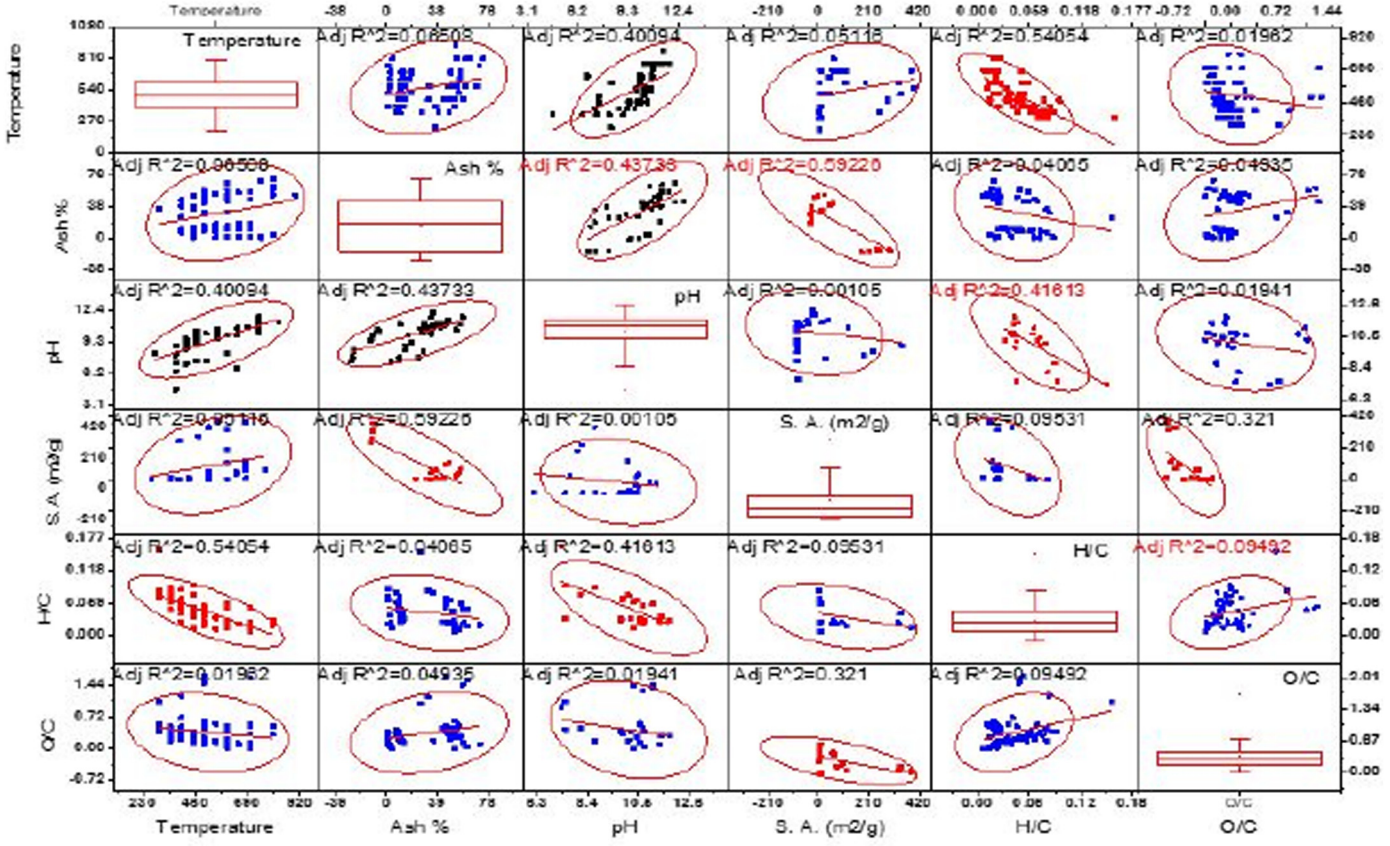

Fig. 7. Scatter matrix of manure-derived biochars. The pyrolysis effects on the physicochemical properties of manure biochar and their interrelations, bivariate pair scatterplots (95% confidence level) with trend lines.

Table 1
Interrelationships and trends of correlation coefficient (r^2) for parameters of biochars.

Parameter of biochars	Types of biochar	Temp (°C)	Ash%	pH	S.A (m^2/g)	H/C	O/C
Correlation coefficient (r^2)							
Temp (°C)	GBC	–					
	SBC						
	HBC						
	MBC						
Ash %	GBC	+0.03	–				
	SBC	+0.01					
	HBC	+0.46					
	MBC	+0.07					
pH	GBC	+0.40	+0.39	–			
	SBC	+0.24	+0.025				
	HBC	+0.41	+0.24				
	MBC	+0.40	+0.44				
S.A (m^2/g)	GBC	+0.28	−0.01	+0.06			
	SBC	+0.35	−0.02	+0.25	–		
	HBC	+0.50	−0.10	+0.44			
	MBC	+0.05	−0.59	−0.001			
H/C	GBC	−0.59	−0.08	−0.71	−0.06		
	SBC	−0.78	−0.01	−0.18	−0.33	–	
	HBC	−0.62	−0.04	−0.21	−0.40		
	MBC	−0.54	−0.04	−0.42	−0.10		
O/C	GBC	−0.44	−0.11	−0.23	−0.002	+0.73	–
	SBC	−0.75	−0.03	−0.06	−0.40	+0.91	
	HBC	−0.40	−0.003	−0.25	−0.13	+0.72	
	MBC	−0.02	−0.04	−0.02	−0.32	+0.10	

Here, Temp - temperature, S.A. - surface area, O/C - oxygen/carbon, H/C - hydrogen/carbon content.

4.8. Adsorption of inorganic contaminants

The sorption of inorganic contaminants, including heavy metal(loid)s, are generally governed by chemisorption including coordination, precipitation, complexation, ion exchange, and electrostatic interactions (Dai et al., 2019; Hale et al., 2013; Hassan et al., 2019; Wang et al., 2020a). Heavy metals are generally adsorbed as a monolayer over the active sites of biochar through physisorption and chemisorption. The adsorption of heavy metals is usually rapid on low pyrolysed biochar due to the predominance of cation exchange reactions, electrostatic interaction, and complexation. In contrast, slow sorption rates were observed with highly pyrolysed biochars (500 °C and 800 °C) due to intra-particle diffusion of cations and anions (Ding et al., 2014), reflecting that adsorption of cations and anions by electrostatic interaction and ion exchange reactions are faster than intra-particle diffusion (Kannan and Sundaram, 2001). Thus, low pyrolysed biochars are therefore suitable for rapid and efficient adsorption of ionic contaminants. Protonation and deprotonation of biochar depend on the isoelectric point of the biochars and individual acid dissociation constants values of the functional groups of biochar (Fiol and Villaescusa, 2009; Kosmulski, 2002; Kosmulski, 2009). The isoelectric point (IEP), and pH of biochar usually depend on the feedstock sources and pyrolysis temperature (Chen et al., 2014a; Li et al., 2017; Yuan et al., 2011).With increasing HTT, pH, and IEP of biochar increased (Banik et al., 2018; Menéndez et al., 1995). Thus, low HTT is suitable for cations sorption, whereas comparatively moderate and high HTT are suitable for anions sorption.

GBC and MBC are suitable feedstock materials for producing biochars for the removal of ionic contaminants due to their high O/C values, despite their lower stability, high ash yield, and subsequently low biochar yield in comparison with HBC and SBC. GBC and MBC have better adsorption performance for ionic contaminants than wood-derived biochar (SBC and HBC) due to the abundance of oxygen-containing functional groups and high CEC. For example, the sorption capacity for Pb^{2+} was found to be 1.84 and 4.25 mg/g onto pinewood (Ahmady-Asbchin and Bahrami) and rice husk (GBC) biochars, respectively (Liu and Zhang, 2009). Similarly, the sorption performance for NH_4^+ was evaluated with biochar derived corn straw, peanut shell, and wheat straw. Of these, the corn straw-derived biochar showed the greatest adsorption capacity as it had the largest CEC (Gai et al., 2014). Therefore, GBC and MBC are good candidates for removal of ionic contaminants. Moreover, MBC has greater efficacy for the sorption of ionic contaminants than GBC due to the presence of alkali metals, which could provide additional active sites for sorption. However, MBC is less suitable as adsorbents for wastewater treatments due to their low surface area, highly alkaline properties, and the highest percentages of ash production. HBC is relatively stable and capable of high aromaticity but has lower polarity than biochars derived from other sources. Therefore, HBC has low efficiency for ionic contaminant removal but high efficiency for removal of organic contaminants. The presence of oxygen-containing functional groups resulting from low-temperature pyrolysis biochar enhanced heavy metals sorption (Gai et al., 2014). With increasing HTT, sorption capacity for ionic contaminants decreased due to a reduction of the affinity among sorbents and sorbates. This was ascribed to aromatization (Gai et al., 2014). When the HTT is increased, biochar surface structure transforms from heterogeneous to homogeneous molecular structures due to the formation of an ordered graphitic structure that is not suitable for sorption of ionic molecules (Fig. 8b). For example, the adsorption capacity for Pb^{2+} by bagasse derived biochar (GBC) decreased from 21 to 6 mg/g as HTT increased from 250 to 600 °C, due to inducing non-polar surface properties and reductions of aliphatic functional groups (Ding et al., 2014).

4.9. Adsorption of organic contaminants

The sorption of organic contaminant onto biochar surfaces is generally controlled by physical sorption mechanisms including van der Waals force, London dipole, hydrophobic interaction, π *stacking*, *partition*, *pore-filling*, *and intra-particle diffusion* (Table 2), where pH has no significant influence (Hopkins and Hawboldt, 2020; Lyu et al., 2018; Wang and Wang, 2019). *Physical sorption* is influenced by surface area, aromaticity, hydrophobicity, and porosity (Hassan et al., 2020; Kupryianchyk et al., 2016). The aromatic carbon structure of biochar is favorable for hydrophobic interactions with organic

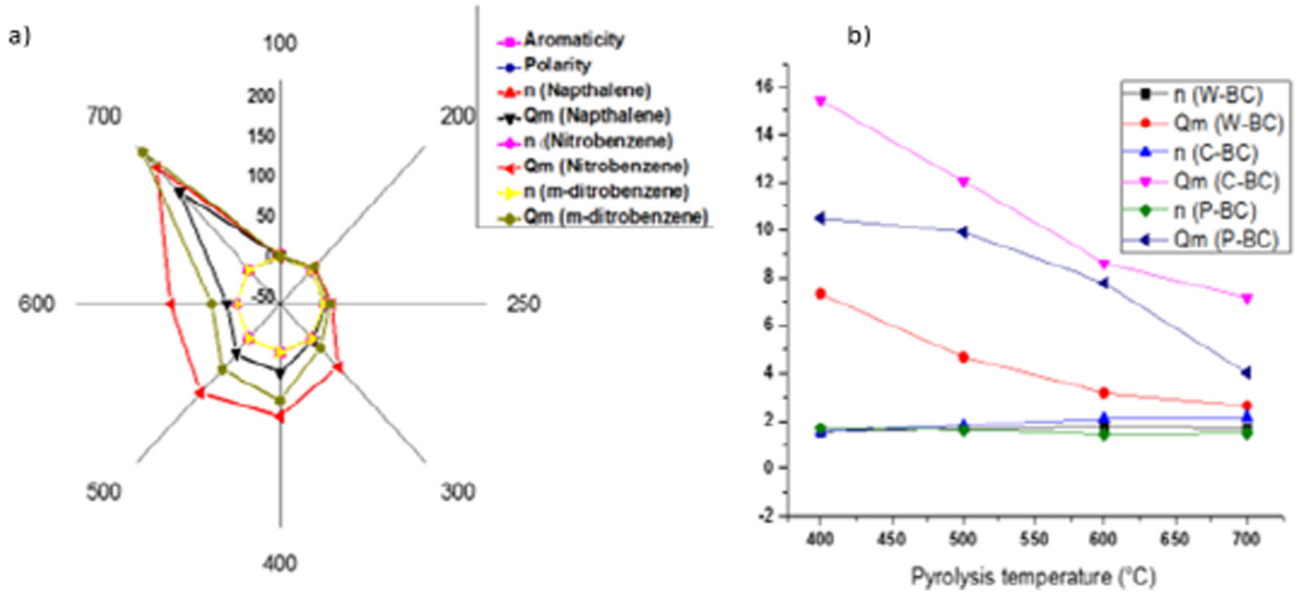

Fig. 8. (a) Interrelationships of sorption parameters for naphthalene, nitrobenzene, and m-dinitrobenzene and thermally modified (100–700 °C) pine needle-derived biochars (Chen et al., 2008); (b) Interrelationships of isotherm parameters of ammonium (NH_4^+) by adsorption on to wheat straw (W-BC), corn straw (C-BC), and peanut-shell (P-BC) derived thermally modified (400–700 °C) biochar (Gai et al., 2014).

contaminants, which can be achieved by high HTT (Hassan et al., 2019). The size of pores increases with pyrolysis temperature and can be readily filled with organic contaminants (Ahmad et al., 2013a; Kang et al., 2018). Recently, Hale and colleagues concluded that the biochar-water partitioning coefficients (K_d values) of neutral organic contaminants are positively correlated with surface area and pyrolysis temperature. In contrast, negative correlations with O/C and H/C values were due to the lack of ion exchange interaction and charge-assisted bonding mechanisms (Fig. S5) (Hale et al., 2016). However, charged organic contaminants can be adsorbed by electrostatic interactions (Fagbayigbo et al., 2017). The sorption of ionic organic contaminants (e.g., PFOS, methylene blue) is influenced by both physical and chemical sorption (Hassan et al., 2020; Lyu et al., 2018). The sorption of naphthalene, nitrobenzene, and m-dinitrobenzene onto thermally modified (100–700 °C) biochars was observed and compared (Fig. 8a). All three organic contaminants had very high sorption affinity with highly pyrolyzed biochar (Chen et al., 2008). Similarly, pine needle-derived biochars were prepared at 300, 500, and 700 °C pyrolysis temperatures to evaluate their performance for the removal of trichloroethylene (TCE) from water (Ahmad et al., 2013b).

Higher sorption density was observed in the most pyrolyzed biochar due to high aromaticity, large surface area, and microporosity. Sorption parameters (Freundlich intensity parameter (n) and Freundlich constant (*Kf*)) were linearly related to the aromaticity of biochar, which is influenced by pyrolysis temperature of biochars (Chen et al., 2008). Low-temperature biochar generally showed partition-dominant sorption, whereas high-temperature biochar demonstrated adsorption-dominant sorption for non-ionic organic contaminants (Ahmad et al., 2013b). Adsorption and partition depend on both the carbonized and non-carbonized fractions of biochars (Chen et al., 2008; Uchimiya et al., 2010b). For example, naphthalene was adsorbed onto carbonized biochar at higher HTT (500–700 °C) by adsorption, whereas it partitioned with well-hydrated non-carbonized

Table 2
Temperature effects on biochar physiochemical properties and their relationships with organic and inorganic contaminant removal from wastewater.

Pyrolysis temperature (°C)	Low pyrolysis (100 °C – 300 °C)	Mild pyrolysis (300 °C - 500 °C)	High pyrolysis (500 °C–700/800 °C)
Structural degradation (Fang et al., 2020; Hassan et al., 2019; Lian and Xing, 2017; Liu et al., 2017; Ranzi et al., 2008)	Cellulose and hemicellulose start to decompose	Lignin starts to decompose along with cellulose and hemicellulose	Formation of benzene polymer, carbon ring structure, and high ash production
Active sites for sorption (Hassan et al., 2019; Lian and Xing, 2017; Uchimiya et al., 2011; Yang et al., 2019; Zhang et al., 2017; Zhao et al., 2020)	-C-C-, -C=C-, -C-O-, -O-H	COOH-, COH-, OH-,	COOH-, benzene ring, aromatic structure, and non-polarity
pH of biochar	Slightly acidic to acidic	Slightly alkaline to mildly alkaline	Mild to highly alkaline
Adsorption performance (Chen et al., 2008; Chen et al., 2012b; Hu et al., 2020; Neris et al., 2019; Uchimiya et al., 2011; Xiao et al., 2018)	Higher for ionic contaminants but lower for organics	Relatively lower for ionic but higher for organic contaminants	Very high (max.) for organic contaminants and lowest for ionic molecules
Inorganic contaminants adsorption mechanism (Bair et al., 2016; Cao et al., 2009; Chen et al., 2011; Chen et al., 2015; Dong et al., 2013; Fang et al., 2014; Oliveira et al., 2017; Qi et al., 2017a; Qi et al., 2018; Qi et al., 2017b; Qian and Chen, 2014; Shen et al., 2017; Uchimiya et al., 2010a; Uchimiya et al., 2011; Xiao et al., 2018)	Complexation, electrostatic interaction, and ion exchange	Complexation, hydrogen bonding, electrostatic interaction, and ion exchanges	Co-precipitation, ion exchanges, precipitation, and co-ordination bonding
Organic contaminants adsorption mechanism (Ashoori et al., 2019; Bair et al., 2016; Burnell et al., n.d.; Chen et al., 2019; Hassan et al., 2020; Lattao et al., 2014; Lian and Xing, 2017; Oberoi et al., 2019; Pignatello et al., 2017; Teixidó et al., 2011; Tomul et al., 2020; Ulrich et al., 2015; Ulrich et al., 2017; Wang et al., 2015a; Xiao et al., 2018; Xiao et al., 2017)	Partition, hydration, H-bond, and hydrophobic interaction (low)	Hydrogen bonding, partition, hydrophobic interaction, and π-bond	Pore filling and hydrophobic interaction, and π- π bond.

biochar at lower HTT (150 °C) (Chen et al., 2012a). The effects of pyrolysis temperature on the removal mechanisms of the organic and inorganic contaminants from wastewater are highlighted below (Table 2).

5. Conclusions and future perspectives

The above discussion on the physicochemical properties of biochar can facilitate the design of biochars for particular applications, such as environmental remediation, soil amendments, and carbon sequestration. This review provides an overview of existing data to facilitate decision making for the end-users of biochar. Some significant outcomes of this review are summarized below:

- The properties of biochar, including surface area, pH, polarity, and stability, are influenced by pyrolysis temperature. The carbon content, surface area, pH, and O/C vs. H/C increase, while biochar yield, H/C, and O/C ratios of biochar decrease with increasing HTT. High pyrolysis temperature can reduce aliphatic and oxygen-containing functional groups and induce aromatic active sites. Therefore, biochars pyrolyzed at high temperature are suitable for adsorption of organic contaminants, whereas biochars pyrolyzed at low temperature are suitable for removal of ionic contaminants. Pyrolysis temperatures also influence adsorption mechanisms. Low pyrolysed biochars generally adsorb inorganic contaminants by electrostatic interaction, ion exchange, and polarity selective interactions. Pore-filling, hydrophobic interaction, and precipitation are the dominant sorption mechanisms for highly pyrolyzed biochar. Solution pH is one of the most dominant factors determining biochar adsorption performance, especially for ionic contaminants. The protonated functional groups generally favor anionic organic and inorganic contaminants, while deprotonated functional groups favor cationic contaminants, including heavy metals.
- Cellulose and hemicellulose transform into low molecular weight carbonaceous species and consequently form aromatic polymers at low HTT, whereas lignin was degrade and transform at comparatively high HTT. The yields of biochars mainly depend on the lignin percentages of feedstocks and pyrolysis temperature. The diversity of functional groups decreases with increasing HTT. With increases of pyrolysis temperature, the polarity of biochar decreased, and consequently, hydrophobicity increased. The stability may vary depending on the types of feedstock and pyrolysis temperature. The sequence of biochar stability against thermal decomposition and volatilization is HBC > SBC > GBC > MBC.
- This article established firm and precise links between the thermal conversion of different types of feedstocks and the properties of resulting biochars. To be specific, GBC and MBC have more oxygen-containing functional groups than the wood-derived biochars (HBC and SBC). On the other hand, wood is suitable for synthesis of highly hydrophobic and aromatic biochar (SBC and HBC) due to high thermal stability in comparison with the grass and manure derived biochars. GBC and MBC are suitable for adsorption of ionic contaminants due to the abundance of functional groups, whereas wood-derived biochar is suitable for adsorption of organic contaminants due to hydrophobic interactions. Furthermore, MBC are less suitable adsorbents for wastewater treatments due to their small surface area, susceptibility to release alkali metals, and higher ash production, in comparison with the other biochars.
- The inorganic minerals phase of biochar also plays a significant role in the adsorption of contaminants. Ionic contaminants can be adsorbed by precipitation, coordination, and ion exchange reactions with the mineral phases of biochar. Additionally, these active sites could perform catalytic degradation of labile organic contaminants from soil and water.

There is limited information on the physiochemical properties of hydrothermally modified biochar, microwave-assisted biochar, and engineered biochar, which should be further investigated for comparison with conventional biochar. Although most of the published research articles focused on single feedstock sources, multiple feedstocks sources should be explored to determine their synergistic or antagonistic effects on the sorption performance for organic and inorganic contaminants. We also suggest that biochar interactions in natural water systems to examine depositional behavior, contaminant transport, aggregation behavior, and toxicity, should be more precisely investigated. To avoid toxicity and long-term desorption, ex situ remediation of wastewater can be considered. Finally, the separation of biochar (e.g., via magnetic biochars) after adsorption and regeneration should be considered to reduce remediation costs. The practical application of biochar for waste management and agricultural use can provide several synergistic benefits, including opening of small businesses, reductions in carbon emissions, and cost-effective remediation of contamination.

Supplementary data to this article can be found online at https://doi.org/10.1016/j.scitotenv.2020.140714.

Declaration of competing interest

The authors declare that they have no known competing financial interests or personal relationships that could have appeared to influence the work reported in this paper.

Acknowledgments

This work was supported by the Global Centre for Environmental Remediation (GCER), University of Newcastle (UON), Australia, and the Cooperative Research Centre for Contamination Assessment and Remediation of the Environment (CRC CARE), Australia. The authors would like to thank Dr. Huiming Zhang (EMX unit, UON) for the characterization (TEM imaging) of the biochar.

References

Abiven, S., Schmidt, M., Lehmann, J., 2014. Biochar by design. Nat. Geosci. 7, 326.
Ahmad, M., Lee, S.S., Oh, S.-E., Mohan, D., Moon, D.H., Lee, Y.H., et al., 2013a. Modeling adsorption kinetics of trichloroethylene onto biochars derived from soybean stover and peanut shell wastes. Environ. Sci. Pollut. Res. 20, 8364–8373.
Ahmad, M., Lee, S.S., Rajapaksha, A.U., Vithanage, M., Zhang, M., Cho, J.S., et al., 2013b. Trichloroethylene adsorption by pine needle biochars produced at various pyrolysis temperatures. Bioresour. Technol. 143, 615–622.
Ahmad, M., Rajapaksha, A.U., Lim, J.E., Zhang, M., Bolan, N., Mohan, D., et al., 2014. Biochar as a sorbent for contaminant management in soil and water: a review. Chemosphere 99, 19–33.
Angin, D., 2013. Effect of pyrolysis temperature and heating rate on biochar obtained from pyrolysis of safflower seed press cake. Bioresour. Technol. 128, 593–597.
Ashoori, N., Teixido, M., Spahr, S., LeFevre, G.H., Sedlak, D.L., Luthy, R.G., 2019. Evaluation of pilot-scale biochar-amended woodchip bioreactors to remove nitrate, metals, and trace organic contaminants from urban stormwater runoff. Water Res. 154, 1–11.
Bair, D.A., Mukome, F.N., Popova, I.E., Ogunyoku, T.A., Jefferson, A., Wang, D., et al., 2016. Sorption of pharmaceuticals, heavy metals, and herbicides to biochar in the presence of biosolids. J. Environ. Qual. 45, 1998–2006.
Banik, C., Lawrinenko, M., Bakshi, S., Laird, D., 2018. Impact of pyrolysis temperature and feedstock on surface charge and functional group chemistry of biochars. Journal of Environment Quality 47.
Beesley, L., Moreno-Jiménez, E., Gomez-Eyles, J.L., Harris, E., Robinson, B., Sizmur, T., 2011. A review of biochars' potential role in the remediation, revegetation and restoration of contaminated soils. Environ. Pollut. 159, 3269–3282.
Budai, A., Wang, L., Gronli, M., Strand, L.T., Antal, M.J., Abiven, S., et al., 2014. Surface properties and chemical composition of corncob and Miscanthus biochars: effects of production temperature and method. J. Agric. Food Chem. 62, 3791–3799.
Burnell S, Planes MT, Sedlak D. Enhanced removal of urban stormwater runoff contaminants using biochar and manganese oxide-coated sand geomedia in a sequential biofiltration system.
Butterfield, B., 2006. The Structure of Wood: Form and Function. Primary Wood Processing. Springer, pp. 1–22.
Cantrell, K.B., Hunt, P.G., Uchimiya, M., Novak, J.M., Ro, K.S., 2012. Impact of pyrolysis temperature and manure source on physicochemical characteristics of biochar. Bioresour. Technol. 107, 419–428.
Cao, X., Ma, L., Gao, B., Harris, W., 2009. Dairy-manure derived biochar effectively sorbs lead and atrazine. Environmental science & technology 43, 3285–3291.
Cao, X., Ro, K.S., Chappell, M., Li, Y., Mao, J., 2010. Chemical structures of swine-manure chars produced under different carbonization conditions investigated by advanced

solid-state 13C nuclear magnetic resonance (NMR) spectroscopy. Energy Fuel 25, 388–397.
Chatterjee, S., Saito, T., 2015. Lignin-derived advanced carbon materials. ChemSusChem 8, 3941–3958.
Chen, B., Chen, Z., 2009. Sorption of naphthalene and 1-naphthol by biochars of orange peels with different pyrolytic temperatures. Chemosphere 76, 127–133.
Chen, B., Zhou, D., Zhu, L., 2008. Transitional adsorption and partition of nonpolar and polar aromatic contaminants by biochars of pine needles with different pyrolytic temperatures. Environmental science & technology 42, 5137–5143.
Chen, X., Chen, G., Chen, L., Chen, Y., Lehmann, J., McBride, M.B., et al., 2011. Adsorption of copper and zinc by biochars produced from pyrolysis of hardwood and corn straw in aqueous solution. Bioresour. Technol. 102, 8877–8884.
Chen, Z., Chen, B., Chiou, C.T., 2012a. Fast and slow rates of naphthalene sorption to biochars produced at different temperatures. Environmental Science & Technology 46, 11104–11111.
Chen, Z., Chen, B., Zhou, D., Chen, W., 2012b. Bisolute sorption and thermodynamic behavior of organic pollutants to biomass-derived biochars at two pyrolytic temperatures. Environmental Science & Technology 46, 12476–12483.
Chen, T., Zhang, Y., Wang, H., Lu, W., Zhou, Z., Zhang, Y., et al., 2014a. Influence of pyrolysis temperature on characteristics and heavy metal adsorptive performance of biochar derived from municipal sewage sludge. Bioresour. Technol. 164, 47–54.
Chen, Z., Xiao, X., Chen, B., Zhu, L., 2014b. Quantification of chemical states, dissociation constants and contents of oxygen-containing groups on the surface of biochars produced at different temperatures. Environmental science & technology 49, 309–317.
Chen, Z., Xiao, X., Chen, B., Zhu, L., 2015. Quantification of chemical states, dissociation constants and contents of oxygen-containing groups on the surface of biochars produced at different temperatures. Environmental Science & Technology 49, 309–317.
Chen, Z., Xiao, X., Xing, B., Chen, B., 2019. pH-dependent sorption of sulfonamide antibiotics onto biochars: sorption mechanisms and modeling. Environ. Pollut. 248, 48–56.
Chun, Y., Sheng, G., Chiou, C.T., Xing, B., 2004. Compositions and sorptive properties of crop residue-derived chars. Environmental science & technology 38, 4649–4655.
Clemente, J.S., Beauchemin, S., Thibault, Y., MacKinnon, T., Smith, D., 2018. Differentiating inorganics in biochars produced at commercial scale using principal component analysis. ACS Omega 3, 6931–6944.
Collard, F.-X., Blin, J., Bensakhria, A., Valette, J., 2012. Influence of impregnated metal on the pyrolysis conversion of biomass constituents. J. Anal. Appl. Pyrolysis 95, 213–226.
Crombie, K., Mašek, O., 2015. Pyrolysis biochar systems, balance between bioenergy and carbon sequestration. GCB Bioenergy 7, 349–361.
Crombie, K., Mašek, O., Sohi, S.P., Brownsort, P., Cross, A., 2013. The effect of pyrolysis conditions on biochar stability as determined by three methods. GCB Bioenergy 5, 122–131.
Dai, Z., Brookes, P.C., He, Y., Xu, J., 2014. Increased agronomic and environmental value provided by biochars with varied physiochemical properties derived from swine manure blended with rice straw. J. Agric. Food Chem. 62, 10623–10631.
Dai, Y., Zhang, N., Xing, C., Cui, Q., Sun, Q., 2019. The adsorption, regeneration and engineering applications of biochar for removal organic pollutants: a review. Chemosphere 223, 12–27.
de Andrade, J.R., Oliveira, M.F., da Silva, M.G.C., Vieira, M.G.A., 2018. Adsorption of pharmaceuticals from water and wastewater using nonconventional low-cost materials: a review. Ind. Eng. Chem. Res. 57, 3103–3127.
Di Blasi, C., Galgano, A., Branca, C., 2009. Influences of the chemical state of alkaline compounds and the nature of alkali metal on wood pyrolysis. Ind. Eng. Chem. Res. 48, 3359–3369.
Ding, W., Dong, X., Ime, I.M., Gao, B., Ma, L.Q., 2014. Pyrolytic temperatures impact lead sorption mechanisms by bagasse biochars. Chemosphere 105, 68–74.
Dong, X., Ma, L.Q., Zhu, Y., Li, Y., Gu, B., 2013. Mechanistic investigation of mercury sorption by Brazilian pepper biochars of different pyrolytic temperatures based on X-ray photoelectron spectroscopy and flow calorimetry. Environmental Science & Technology 47, 12156–12164.
Downie, A., Crosky, A., Munroe, P., 2012. Physical Properties of Biochar. Biochar for Environmental Management. Routledge, pp. 45–64.
Elimelech, M., Phillip, W.A., 2011. The future of seawater desalination: energy, technology, and the environment. Science 333, 712–717.
Elkhalifa, S., Al-Ansari, T., Mackey, H.R., McKay, G., 2019. Food waste to biochars through pyrolysis: a review. Resour. Conserv. Recycl. 144, 310–320.
Fagbayigbo, B.O., Opeolu, B.O., Fatoki, O.S., Akenga, T.A., Olatunji, O.S., 2017. Removal of PFOA and PFOS from aqueous solutions using activated carbon produced from Vitis vinifera leaf litter. Environ. Sci. Pollut. Res. 24, 13107–13120.
Fang, Q., Chen, B., Lin, Y., Guan, Y., 2013. Aromatic and hydrophobic surfaces of wood-derived biochar enhance perchlorate adsorption via hydrogen bonding to oxygen-containing organic groups. Environmental science & technology 48, 279–288.
Fang, Q., Chen, B., Lin, Y., Guan, Y., 2014. Aromatic and hydrophobic surfaces of wood-derived biochar enhance perchlorate adsorption via hydrogen bonding to oxygen-containing organic groups. Environmental Science & Technology 48, 279–288.
Fang, Z., Gao, Y., Bolan, N., Shaheen, S.M., Xu, S., Wu, X., et al., 2020. Conversion of biological solid waste to graphene-containing biochar for water remediation: a critical review. Chem. Eng. J. 390, 124611.
Fiol, N., Villaescusa, I., 2009. Determination of sorbent point zero charge: usefulness in sorption studies. Environ. Chem. Lett. 7, 79–84.
Gai, X., Wang, H., Liu, J., Zhai, L., Liu, S., Ren, T., et al., 2014. Effects of feedstock and pyrolysis temperature on biochar adsorption of ammonium and nitrate. PLoS One 9, e113888.
George, A., Morgan, T.J., Kandiyoti, R., 2014. Pyrolytic reactions of lignin within naturally occurring plant matrices: challenges in biomass pyrolysis modeling due to synergistic effects. Energy Fuel 28, 6918–6927.
Gollehon, N.R., Caswell, M., Ribaudo, M., Kellogg, R.L., Lander, C., Letson, D., 2001. Confined Animal Production and Manure Nutrients.
Guo, J., Chen, B., 2014. Insights on the molecular mechanism for the recalcitrance of biochars: interactive effects of carbon and silicon components. Environmental Science & Technology 48, 9103–9112.
Hagemann, N., Subdiaga, E., Orsetti, S., de la Rosa, J.M., Knicker, H., Schmidt, H.-P., et al., 2018. Effect of biochar amendment on compost organic matter composition following aerobic compositing of manure. Sci. Total Environ. 613, 20–29.
Hale, S.E., Alling, V., Martinsen, V., Mulder, J., Breedveld, G., Cornelissen, G., 2013. The sorption and desorption of phosphate-P, ammonium-N and nitrate-N in cacao shell and corn cob biochars. Chemosphere 91, 1612–1619.
Hale, S.E., Arp, H.P.H., Kupryianchyk, D., Cornelissen, G., 2016. A synthesis of parameters related to the binding of neutral organic compounds to charcoal. Chemosphere 144, 65–74.
Han, L., Ro, K.S., Wang, Y., Sun, K., Sun, H., Libra, J.A., et al., 2018. Oxidation resistance of biochars as a function of feedstock and pyrolysis condition. Sci. Total Environ. 616, 335–344.
Harvey, O.R., Herbert, B.E., Rhue, R.D., Kuo, L.-J., 2011. Metal interactions at the biochar-water interface: energetics and structure-sorption relationships elucidated by flow adsorption microcalorimetry. Environmental science & technology 45, 5550–5556.
Hassan, M., Naidu, R., Du, J., Liu, Y., Qi, F., 2019. Critical review of magnetic biosorbents: their preparation, application, and regeneration for wastewater treatment. Sci. Total Environ. 702, 134893.
Hassan, M., Liu, Y., Naidu, R., Du, J., Qi, F., 2020. Adsorption of Perfluorooctane sulfonate (PFOS) onto metal oxides modified biochar. Environmental Technology & Innovation 19, 100816.
Hopkins, D., Hawboldt, K., 2020. Biochar for the removal of metals from solution: a review of lignocellulosic and novel marine feedstocks. Journal of Environmental Chemical Engineering 8, 103975.
Hu, X., Zhang, X., Ngo, H.H., Guo, W., Wen, H., Li, C., et al., 2020. Comparison study on the ammonium adsorption of the biochars derived from different kinds of fruit peel. Sci. Total Environ. 707, 135544.
Jung, K.-W., Kim, K., Jeong, T.-U., Ahn, K.-H., 2016. Influence of pyrolysis temperature on characteristics and phosphate adsorption capability of biochar derived from waste-marine macroalgae (Undaria pinnatifida roots). Bioresour. Technol. 200, 1024–1028.
Kan, T., Strezov, V., Evans, T.J., 2016. Lignocellulosic biomass pyrolysis: a review of product properties and effects of pyrolysis parameters. Renew. Sust. Energ. Rev. 57, 1126–1140.
Kang, S., Jung, J., Choe, J.K., Ok, Y.S., Choi, Y., 2018. Effect of biochar particle size on hydrophobic organic compound sorption kinetics: applicability of using representative size. Sci. Total Environ. 619, 410–418.
Kannan, N., Sundaram, M.M., 2001. Kinetics and mechanism of removal of methylene blue by adsorption on various carbons—a comparative study. Dyes Pigments 51, 25–40.
Karunanithi, R., Ok, Y.S., Dharmarajan, R., Ahmad, M., Seshadri, B., Bolan, N., et al., 2017. Sorption, kinetics and thermodynamics of phosphate sorption onto soybean stover derived biochar. Environmental Technology & Innovation 8, 113–125.
Keiluweit, M., Nico, P.S., Johnson, M.G., Kleber, M., 2010. Dynamic molecular structure of plant biomass-derived black carbon (biochar). Environmental science & technology 44, 1247–1253.
Kloss, S., Zehetner, F., Dellantonio, A., Hamid, R., Ottner, F., Liedtke, V., et al., 2012. Characterization of slow pyrolysis biochars: effects of feedstocks and pyrolysis temperature on biochar properties. J. Environ. Qual. 41, 990–1000.
Kosmulski, M., 2002. The pH-dependent surface charging and the points of zero charge. J. Colloid Interface Sci. 253, 77–87.
Kosmulski, M., 2009. Surface Charging and Points of Zero Charge. vol 145. CRC Press.
Kupryianchyk, D., Hale, S., Zimmerman, A.R., Harvey, O., Rutherford, D., Abiven, S., et al., 2016. Sorption of hydrophobic organic compounds to a diverse suite of carbonaceous materials with emphasis on biochar. Chemosphere 144, 879–887.
Lattao, C., Cao, X., Mao, J., Schmidt-Rohr, K., Pignatello, J.J., 2014. Influence of molecular structure and adsorbent properties on sorption of organic compounds to a temperature series of wood chars. Environmental Science & Technology 48, 4790–4798.
Lehmann, J., 2007. A handful of carbon. Nature 447, 143.
Lehmann, J., Joseph, S., 2015. Biochar for Environmental Management: Science, Technology and Implementation. Routledge.
Lehmann, J., Kleber, M., 2015. The contentious nature of soil organic matter. Nature 528, 60.
Lehmann, J., Gaunt, J., Rondon, M., 2006. Bio-char sequestration in terrestrial ecosystems – a review. Mitig. Adapt. Strateg. Glob. Chang. 11, 403–427.
Leng, L., Huang, H., Li, H., Li, J., Zhou, W., 2018. Biochar stability assessment methods: a review. Sci. Total Environ. 647, 210–222.
Leng, L., Huang, H., Li, H., Li, J., Zhou, W., 2019. Biochar stability assessment methods: a review. Sci. Total Environ. 647, 210–222.
Li, H., Dong, X., da Silva, E.B., de Oliveira, L.M., Chen, Y., Ma, L.Q., 2017. Mechanisms of metal sorption by biochars: biochar characteristics and modifications. Chemosphere 178, 466–478.
Lian, F., Xing, B., 2017. Black carbon (biochar) in water/soil environments: molecular structure, sorption, stability, and potential risk. Environmental Science & Technology 51, 13517–13532.
Liu, Z., Zhang, F.-S., 2009. Removal of lead from water using biochars prepared from hydrothermal liquefaction of biomass. J. Hazard. Mater. 167, 933–939.
Liu, H., Zhang, L., Han, Z., Xie, B., Wu, S., 2013a. The effects of leaching methods on the combustion characteristics of rice straw. Biomass Bioenergy 49, 22–27.
Liu, W.-J., Jiang, H., Tian, K., Ding, Y.-W., Yu, H.-Q., 2013b. Mesoporous carbon stabilized MgO nanoparticles synthesized by pyrolysis of $MgCl_2$ preloaded waste biomass for highly efficient CO_2 capture. Environmental science & technology 47, 9397–9403.
Liu, W.-J., Jiang, H., Yu, H.-Q., 2015. Development of biochar-based functional materials: toward a sustainable platform carbon material. Chem. Rev. 115, 12251–12285.

Liu, Y., Naidu, R., Ming, H., Dharmarajan, R., Du, J., 2016. Effects of thermal treatments on the characterisation and utilisation of red mud with sawdust additive. Waste Manag. Res. 34, 518–526.
Liu, W.-J., Li, W.-W., Jiang, H., Yu, H.-Q., 2017. Fates of chemical elements in biomass during its pyrolysis. Chem. Rev. 117, 6367–6398.
Luo, L., Xu, C., Chen, Z., Zhang, S., 2015. Properties of biomass-derived biochars: combined effects of operating conditions and biomass types. Bioresour. Technol. 192, 83–89.
Lyu, H., Gao, B., He, F., Zimmerman, A.R., Ding, C., Tang, J., et al., 2018. Experimental and modeling investigations of ball-milled biochar for the removal of aqueous methylene blue. Chem. Eng. J. 335, 110–119.
McBeath, A.V., Smernik, R.J., Krull, E.S., Lehmann, J., 2014. The influence of feedstock and production temperature on biochar carbon chemistry: a solid-state ^{13}C NMR study. Biomass Bioenergy 60, 121–129.
Menéndez, J.A., Illán-Gómez, M.J., Leon, Y., Leon, C., Radovic, L., 1995. On the difference between the isoelectric point and the point of zero charge of carbons. Carbon 33, 1655–1657.
Mohanty, S.K., Valenca, R., Berger, A.W., Yu, I.K.M., Xiong, X., Saunders, T.M., et al., 2018. Plenty of room for carbon on the ground: potential applications of biochar for stormwater treatment. Sci. Total Environ. 625, 1644–1658.
Montgomery, M.A., Elimelech, M., 2007. Water and sanitation in developing countries: including health in the equation. Environmental Science & Technology 41, 17–24.
Morales, V.L., Pérez-Reche, F.J., Hapca, S.M., Hanley, K.L., Lehmann, J., Zhang, W., 2015. Reverse engineering of biochar. Bioresour. Technol. 183, 163–174.
Mukome, F.N., Zhang, X., Silva, L.C., Six, J., Parikh, S.J., 2013. Use of chemical and physical characteristics to investigate trends in biochar feedstocks. J. Agric. Food Chem. 61, 2196–2204.
Neris, J.B., Luzardo, F.H.M., da Silva, E.G.P., Velasco, F.G., 2019. Evaluation of adsorption processes of metal ions in multi-element aqueous systems by lignocellulosic adsorbents applying different isotherms: a critical review. Chem. Eng. J. 357, 404–420.
Oberoi, A.S., Jia, Y., Zhang, H., Khanal, S.K., Lu, H., 2019. Insights into the fate and removal of antibiotics in engineered biological treatment systems: a critical review. Environmental Science & Technology 53, 7234–7264.
Oliveira, F.R., Patel, A.K., Jaisi, D.P., Adhikari, S., Lu, H., Khanal, S.K., 2017. Environmental application of biochar: current status and perspectives. Bioresour. Technol. 246, 110–122.
Parham, R.A., Gray, R.L., 1984. Formation and Structure of Wood. ACS Publications.
Pariyar, P., Kumari, K., Jain, M.K., Jadhao, P.S., 2020. Evaluation of change in biochar properties derived from different feedstock and pyrolysis temperature for environmental and agricultural application. Sci. Total Environ. 713, 136433.
Patel, M., Kumar, R., Kishor, K., Mlsna, T., Pittman, C.U., Mohan, D., 2019. Pharmaceuticals of emerging concern in aquatic systems: chemistry, occurrence, effects, and removal methods. Chem. Rev. 119, 3510–3673.
Peters, B., 2011. Prediction of pyrolysis of pistachio shells based on its components hemicellulose, cellulose and lignin. Fuel Process. Technol. 92, 1993–1998.
Petrov, D., Tunega, D., Gerzabek, M.H., Oostenbrink, C., 2017. Molecular dynamics simulations of the standard leonardite humic acid: microscopic analysis of the structure and dynamics. Environmental Science & Technology 51, 5414–5424.
Pignatello, J.J., Mitch, W.A., Xu, W., 2017. Activity and reactivity of pyrogenic carbonaceous matter toward organic compounds. Environmental Science & Technology 51, 8893–8908.
Qi, F., Dong, Z., Lamb, D., Naidu, R., Bolan, N.S., Ok, Y.S., et al., 2017a. Effects of acidic and neutral biochars on properties and cadmium retention of soils. Chemosphere 180, 564–573.
Qi, F., Yan, Y., Lamb, D., Naidu, R., Bolan, N.S., Liu, Y., et al., 2017b. Thermal stability of biochar and its effects on cadmium sorption capacity. Bioresour. Technol. 246, 48–56.
Qi, F., Lamb, D., Naidu, R., Bolan, N.S., Yan, Y., Ok, Y.S., et al., 2018. Cadmium solubility and bioavailability in soils amended with acidic and neutral biochar. Sci. Total Environ. 610, 1457–1466.
Qian, L., Chen, B., 2013. Dual role of biochars as adsorbents for aluminum: the effects of oxygen-containing organic components and the scattering of silicate particles. Environmental science & technology 47, 8759–8768.
Qian, L., Chen, B., 2014. Interactions of aluminum with biochars and oxidized biochars: implications for the biochar aging process. J. Agric. Food Chem. 62, 373–380.
Qu, T., Guo, W., Shen, L., Xiao, J., Zhao, K., 2011. Experimental study of biomass pyrolysis based on three major components: hemicellulose, cellulose, and lignin. Ind. Eng. Chem. Res. 50, 10424–10433.
Rajaganapathy, V., Xavier, F., Sreekumar, D., Mandal, P., 2011. Heavy metal contamination in soil, water and fodder and their presence in livestock and products: a review. J. Environ. Sci. Technol. 4, 234–249.
Ranzi, E., Cuoci, A., Faravelli, T., Frassoldati, A., Migliavacca, G., Pierucci, S., et al., 2008. Chemical kinetics of biomass pyrolysis. Energy Fuel 22, 4292–4300.
Reyhanitabar, A., Frahadi, E., Ramezanzadeh, H., Oustan, S., 2020. Effect of pyrolysis temperature and feedstock sources on physicochemical characteristics of biochar. J. Agric. Sci. Technol. 22, 547–561.
Rondon, M.A., Lehmann, J., Ramírez, J., Hurtado, M., 2007. Biological nitrogen fixation by common beans (Phaseolus vulgaris L.) increases with bio-char additions. Biol. Fertil. Soils 43, 699–708.
Ronsse, F., Van Hecke, S., Dickinson, D., Prins, W., 2013. Production and characterization of slow pyrolysis biochar: influence of feedstock type and pyrolysis conditions. GCB Bioenergy 5, 104–115.
Samsuri, A.W., Sadegh-Zadeh, F., Seh-Bardan, B.J., 2013. Adsorption of as (III) and as (V) by Fe coated biochars and biochars produced from empty fruit bunch and rice husk. Journal of Environmental Chemical Engineering 1, 981–988.
Shannon, M.A., Bohn, P.W., Elimelech, M., Georgiadis, J.G., Mariñas, B.J., Mayes, A.M., 2008. Science and technology for water purification in the coming decades. Nature 452, 301–310.
Sharma, R.K., Wooten, J.B., Baliga, V.L., Lin, X., Geoffrey Chan, W., Hajaligol, M.R., 2004. Characterization of chars from pyrolysis of lignin. Fuel 83, 1469–1482.
Shen, D.K., Gu, S., 2009. The mechanism for thermal decomposition of cellulose and its main products. Bioresour. Technol. 100, 6496–6504.
Shen, Y., Zhao, P., Shao, Q., Ma, D., Takahashi, F., Yoshikawa, K., 2014. In-situ catalytic conversion of tar using rice husk char-supported nickel-iron catalysts for biomass pyrolysis/gasification. Appl. Catal. B Environ. 152, 140–151.
Shen, Z., Zhang, Y., Jin, F., McMillan, O., Al-Tabbaa, A., 2017. Qualitative and quantitative characterisation of adsorption mechanisms of lead on four biochars. Sci. Total Environ. 609, 1401–1410.
Singh, S., Kumar, V., Datta, S., Dhanjal, D.S., Sharma, K., Samuel, J., et al., 2020. Current advancement and future prospect of biosorbents for bioremediation. Sci. Total Environ. 709, 135895.
Sørmo, E., Silvani, L., Thune, G., Gerber, H., Schmidt, H.P., Smebye, A.B., et al., 2020. Waste timber pyrolysis in a medium-scale unit: emission budgets and biochar quality. Sci. Total Environ. 718, 137335.
Spokas, K.A., 2010. Review of the stability of biochar in soils: predictability of O: C molar ratios. Carbon Management 1, 289–303.
Sun, K., Kang, M., Ro, K.S., Libra, J.A., Zhao, Y., Xing, B., 2016. Variation in sorption of propiconazole with biochars: the effect of temperature, mineral, molecular structure, and nano-porosity. Chemosphere 142, 56–63.
Tag, A.T., Duman, G., Ucar, S., Yanik, J., 2016. Effects of feedstock type and pyrolysis temperature on potential applications of biochar. J. Anal. Appl. Pyrolysis 120, 200–206.
Teixidó, M., Pignatello, J.J., Beltrán, J.L., Granados, M., Peccia, J., 2011. Speciation of the ionizable antibiotic sulfamethazine on black carbon (biochar). Environmental science & technology 45, 10020–10027.
Tomul, F., Arslan, Y., Kabak, B., Trak, D., Kendüzler, E., Lima, E.C., et al., 2020. Peanut shells-derived biochars prepared from different carbonization processes: comparison of characterization and mechanism of naproxen adsorption in water. Sci. Total Environ. 726, 137828.
Tripathi, M., Sahu, J.N., Ganesan, P., 2016. Effect of process parameters on production of biochar from biomass waste through pyrolysis: a review. Renew. Sust. Energ. Rev. 55, 467–481.
Tzvelev, N., 1989. The system of grasses (Poaceae) and their evolution. Bot. Rev. 55, 141–203.
Uchimiya, M., Lima, I.M., Thomas Klasson, K., Chang, S., Wartelle, L.H., Rodgers, J.E., 2010a. Immobilization of heavy metal ions (CuII, CdII, NiII, and PbII) by broiler litter-derived biochars in water and soil. J. Agric. Food Chem. 58, 5538–5544.
Uchimiya, M., Wartelle, L.H., Lima, I.M., Klasson, K.T., 2010b. Sorption of deisopropylatrazine on broiler litter biochars. J. Agric. Food Chem. 58, 12350–12356.
Uchimiya, M., Wartelle, L.H., Klasson, K.T., Fortier, C.A., Lima, I.M., 2011. Influence of pyrolysis temperature on biochar property and function as a heavy metal sorbent in soil. J. Agric. Food Chem. 59, 2501–2510.
Ulrich, B.A., Im, E.A., Werner, D., Higgins, C.P., 2015. Biochar and activated carbon for enhanced trace organic contaminant retention in stormwater infiltration systems. Environmental science & technology 49, 6222–6230.
Ulrich, B.A., Vignola, M., Edgehouse, K., Werner, D., Higgins, C.P., 2017. Organic carbon amendments for enhanced biological attenuation of trace organic contaminants in biochar-amended stormwater biofilters. Environmental science & technology 51, 9184–9193.
Wan, X., Li, C., Parikh, S.J., 2020. Simultaneous removal of arsenic, cadmium, and lead from soil by iron-modified magnetic biochar. Environ. Pollut. 261, 114157.
Wang, J., Wang, S., 2019. Preparation, modification and environmental application of biochar: a review. J. Clean. Prod. 227, 1002–1022.
Wang, Y., Hu, Y., Zhao, X., Wang, S., Xing, G., 2013. Comparisons of biochar properties from wood material and crop residues at different temperatures and residence times. Energy Fuel 27, 5890–5899.
Wang, D., Mukome, F.N., Yan, D., Wang, H., Scow, K.M., Parikh, S.J., 2015a. Phenylurea herbicide sorption to biochars and agricultural soil. J. Environ. Sci. Health B 50, 544–551.
Wang, H., Gao, B., Wang, S., Fang, J., Xue, Y., Yang, K., 2015b. Removal of Pb (II), Cu (II), and Cd (II) from aqueous solutions by biochar derived from KMnO4 treated hickory wood. Bioresour. Technol. 197, 356–362.
Wang, Y.-Y., Jing, X.-R., Li, L.-L., Liu, W.-J., Tong, Z.-H., Jiang, H., 2016. Biotoxicity evaluations of three typical biochars using a simulated system of fast pyrolytic biochar extracts on organisms of three kingdoms. ACS Sustain. Chem. Eng. 5, 481–488.
Wang, L., Wang, Y., Ma, F., Tankpa, V., Bai, S., Guo, X., et al., 2019a. Mechanisms and reutilization of modified biochar used for removal of heavy metals from wastewater: a review. Sci. Total Environ. 668, 1298–1309.
Wang, Y., Xiao, X., Xu, Y., Chen, B., 2019b. Environmental effects of silicon within biochar (sichar) and carbon-silicon coupling mechanisms: a critical review. Environ. Sci. Technol. 53, 13570–13582.
Wang, S., Kwak, J.-H., Islam, M.S., Naeth, M.A., Gamal El-Din, M., Chang, S.X., 2020a. Biochar surface complexation and Ni(II), Cu(II), and Cd(II) adsorption in aqueous solutions depend on feedstock type. Sci. Total Environ. 712, 136538.
Wang, Z., Bakshi, S., Li, C., Parikh, S.J., Hsieh, H.-S., Pignatello, J.J., 2020b. Modification of pyrogenic carbons for phosphate sorption through binding of a cationic polymer. J. Colloid Interface Sci. 579, 258–268.
Weber, K., Quicker, P., 2018. Properties of biochar. Fuel 217, 240–261.
Wiedemeier, D.B., Abiven, S., Hockaday, W.C., Keiluweit, M., Kleber, M., Masiello, C.A., et al., 2015. Aromaticity and degree of aromatic condensation of char. Org. Geochem. 78, 135–143.
Wiedenhoeft, A., 2010. Structure and function of wood. Wood handbook: Wood as an engineering material: chapter 3. Centennial Ed. General Technical Report FPL; GTR-190. US Dept. of Agriculture, Forest Service, Forest Products Laboratory, Madison, WI (p. 3.1-3.18. 2010; 190: 3.1-3.18).

Wu, J., Li, Z., Huang, D., Liu, X., Tang, C., Parikh, S.J., et al., 2020. A novel calcium-based magnetic biochar is effective in stabilization of arsenic and cadmium co-contamination in aerobic soils. J. Hazard. Mater. 387, 122010.

Xiao, X., Chen, B., Zhu, L., 2014. Transformation, morphology, and dissolution of silicon and carbon in rice straw-derived biochars under different pyrolytic temperatures. Environmental Science & Technology 48, 3411–3419.

Xiao, X., Chen, Z., Chen, B., 2016. H/C atomic ratio as a smart linkage between pyrolytic temperatures, aromatic clusters and sorption properties of biochars derived from diverse precursory materials. Sci. Rep. 6, 22644.

Xiao, X., Ulrich, B.A., Chen, B., Higgins, C.P., 2017. Sorption of poly-and perfluoroalkyl substances (PFASs) relevant to aqueous film-forming foam (AFFF)-impacted groundwater by biochars and activated carbon. Environmental science & technology 51, 6342–6351.

Xiao, X., Chen, B., Chen, Z., Zhu, L., Schnoor, J.L., 2018. Insight into multiple and multilevel structures of biochars and their potential environmental applications: a critical review. Environmental science & technology 52, 5027–5047.

Yaashikaa, P., Kumar, P.S., Varjani, S.J., Saravanan, A., 2019. Advances in production and application of biochar from lignocellulosic feedstocks for remediation of environmental pollutants. Bioresour. Technol. 122030.

Yan, J., Han, L., Gao, W., Xue, S., Chen, M., 2015. Biochar supported nanoscale zerovalent iron composite used as persulfate activator for removing trichloroethylene. Bioresour. Technol. 175, 269–274.

Yang, H., Yan, R., Chen, H., Lee, D.H., Zheng, C., 2007a. Characteristics of hemicellulose, cellulose and lignin pyrolysis. Fuel 86, 1781–1788.

Yang, H., Yan, R., Chen, H., Lee, D.H., Zheng, C., 2007b. Characteristics of hemicellulose, cellulose and lignin pyrolysis. Fuel 86, 1781–1788.

Yang, X., Wan, Y., Zheng, Y., He, F., Yu, Z., Huang, J., et al., 2019. Surface functional groups of carbon-based adsorbents and their roles in the removal of heavy metals from aqueous solutions: a critical review. Chem. Eng. J. 366, 608–621.

Yuan, J.-H., Xu, R.-K., Zhang, H., 2011. The forms of alkalis in the biochar produced from crop residues at different temperatures. Bioresour. Technol. 102, 3488–3497.

Zhang, M., Gao, B., Yao, Y., Xue, Y., Inyang, M., 2012. Synthesis of porous MgO-biochar nanocomposites for removal of phosphate and nitrate from aqueous solutions. Chem. Eng. J. 210, 26–32.

Zhang, Y., Ma, Z., Zhang, Q., Wang, J., Ma, Q., Yang, Y., et al., 2017. Comparison of the physicochemical characteristics of bio-char pyrolyzed from moso bamboo and rice husk with different pyrolysis temperatures. BioResources 12, 4652–4669.

Zhang, Z., Zhu, Z., Shen, B., Liu, L., 2019. Insights into biochar and hydrochar production and applications: a review. Energy 171, 581–598.

Zhang, W., Du, W., Wang, F., Xu, H., Zhao, T., Zhang, H., et al., 2020a. Comparative study on Pb2+ removal from aqueous solutions using biochars derived from cow manure and its vermicompost. Sci. Total Environ. 716, 137108.

Zhang, X., Zhang, Y., Ngo, H.H., Guo, W., Wen, H., Zhang, D., et al., 2020b. Characterization and sulfonamide antibiotics adsorption capacity of spent coffee grounds based biochar and hydrochar. Sci. Total Environ. 716, 137015.

Zhao, L., Cao, X., Mašek, O., Zimmerman, A., 2013. Heterogeneity of biochar properties as a function of feedstock sources and production temperatures. J. Hazard. Mater. 256-257, 1–9.

Zhao, M., Dai, Y., Zhang, M., Feng, C., Qin, B., Zhang, W., et al., 2020. Mechanisms of Pb and/or Zn adsorption by different biochars: biochar characteristics, stability, and binding energies. Sci. Total Environ. 717, 136894.